THE ASTROPHYSICAL JOURNAL, 318:823–843, 1987 July 15

THE ATMOSPHERES OF T TAURI STARS. I. HIGH-RESOLUTION CALIBRATED OBSERVATIONS OF MODERATELY ACTIVE STARS[1]

ULRICH FINKENZELLER[2] AND GIBOR BASRI
Astronomy Department, University of California, Berkeley
Received 1986 September 10; accepted 1986 December 29

ABSTRACT

Because of their complex and variable nature, a proper theoretical treatment of T Tauri atmospheres requires comprehensive spectral information at a variety of resolutions and wavelengths to be gathered together. The material presented constitutes the most comprehensive observational treatment to date. Calibrated optical spectra from 3700 to 8700 Å with high resolution and signal-to-noise ratio have been obtained quasi-simultaneously for three pairs of cool low- and intermediate-activity southern T Tauri stars and one G2 T Tauri star with well-defined photospheric spectra. Together with observations of spectral standards, these are used to obtain spectral types, reddening corrections, radial velocities, $v \sin i$, and in combination with near-IR and *IRAS* data, photospheric and systemic luminosities. From positions in the H-R diagram, we determine the mass, radius, and surface gravity for each object. Surface fluxes in the emission lines are discussed. For all targets, ratio or difference plots versus appropriate standards are analyzed and show that important features of T Tauri spectra are clearly chromospheric. This method is also useful in analyzing nonradiative heating in the lower atmosphere.

From these data we conclude the following:

1. In addition to emission in the lines of Ca II and the Balmer series, T Tauri stars of spectral types G to early M with low activity show increased emission in the cores of the Mg I B, Ca I, Fe I multiplets 41, 42, 43, and other lines. These lines mark the onset of nonradiative heating in their atmospheres. The same transitions are also seen in the solar chromosphere.

2. All Balmer line profiles for a given star closely resemble each other. At Hα there are four stars with evidence for redshifted absorption. Three stars show clear evidence of blueshifted absorption, and three show marginal evidence for this. In two cases there is obvious absorption both redward and bluward in Hα and Na D. The objects with redhifted features are only marginally reddened and have small emission line strengths. We conclude that this phenomenon is not restricted to active T Tauri stars with very opaque envelopes and that these profiles cannot be explained by simple flow models. Although Hβ appears to be stronger in the cooler stars, examination of surface fluxes shows that the Balmer decrement is actually quite similar for all the stars.

3. The Ca II line profiles are narrow and symmetric with one exception (Sz 98). A correlation is found between Ca II and Hα surface flux, indicating that a common physical process may be responsible for activity from the lower atmosphere to the outer envelope. No correlation is found between He I 5876 and Ca II or Hα line strength, but He I becomes stronger with decreasing effective temperature. This is apparently largely a contrast effect. Our sample shows a decrease of Li I 6707 equivalent width with increasing Ca II K surface flux, but there is also a correlation of lithium with effective temperature.

4. Luminosities obtained by integrating the total observed optical, near- and far-infrared flux, and by evaluating the dereddened photospheric stellar spectra alone, indicate that two targets (Sz 98, Sz 65) may have a separate source which contributes to their IR excess. The IR flux distribution of the remaining objects is more typical of visible photon redistribution. The three objects with the largest $v \sin i$ values are the most reddened ones. These points may be indirect evidence of disks around these relatively less active pre–main-sequence stars.

Subject headings: spectrophotometry — stars: chromospheres — stars: emission-line — stars: pre–main-sequence

I. INTRODUCTION

In the last two decades considerable progress has been made toward a better understanding of the various processes associated with star formation. There is little doubt today that T Tauri stars represent young stellar objects no older than 10^5–10^7 yr which display a large variety of associated stellar activity. From numerous studies at both high (e.g., Hartmann 1982; Ulrich and Knapp 1985; Mundt 1984; or Appenzeller, Jankovics, and Jetter 1986) and low resolution (e.g., Cohen and Kuhi 1979) in a wide wavelength range the general appearance of young stellar objects is qualitatively well understood today. At the same time our knowledge concerning stellar activity in main-sequence stars has improved considerably. Both innovative theoretical concepts and new observational material has provided a much better view of the physical processes that are responsible.

The interest of most observers of T Tauri stars has focused primarily on the brightest objects, characterized by violent

[1] Based on observations collected at the European Southern Observatory, La Silla, Chile.

[2] Feodor-Lynen Fellow, Alexander von Humboldt Foundation.

activity with complex, emission line–rich spectrograms. The large optical depth of the outer atmosphere in these stars usually does not allow an unobscured view down to the stellar photospheres where the stellar activity originates. Detailed interpretation of such observations is hampered by the lack of a firm conceptual framework on which to base theoretical analysis. In this contribution we report on initial results of a study aimed specifically on low-activity T Tauri stars with "transparent" atmospheres and unambiguously classifiable photospheric spectra. To really understand the physical state of these complex systems requires a large effort with model stellar atmospheres and detailed radiative transfer calculations. We have gathered the data necessary for such an effort and plan to report on it in later papers in this series. We concentrate here on a careful discussion of the overall appearance of these systems and point out the degree to which the phenomena observed can be related to what is known from either the more active T Tauri stars or the more quiet older active main-sequence stars.

After describing the observational approach in § II, we discuss the determination of the stellar parameters in § III. This includes discussion of the treatment of interstellar/circumstellar reddening and the evaluation of the bolometric luminosity. In § IV we discuss line profile strengths, shapes, and shifts for particular objects. The comparison of this material with nonactive main sequence stars of similar spectral type follows in § V.

II. TARGET SELECTION AND OBSERVATIONS

Guided by the rule that physical processes can be most easily analyzed in their least complex manifestation, we have chosen seven low to intermediately active T Tauri stars from the low-resolution spectral catalog of Appenzeller, Jankovics, and Krautter (1983). In their work, initial determinations of spectral type Hα equivalent width, and a lower estimate of L are given. Further information can also be found in the original list of Schwartz (1977). The selected targets consist of pairs of spectral type K2, K7–M0, and M0 (with the exception of Sz 19, a single object of type G2) which are almost identical in most parameters except activity level, as referenced by the Hα line strength (see Tables 1 and 2). Together with a set of standard stars chosen to match the T Tauri stars in $T_{\rm eff}$ and L, we are in position to perform a differential activity analysis from the main sequence into the pre–main-sequence domain by extrapolating proven diagnostic methods from quiet to moderately active objects.

Due to the complex nature of the problems inherent in analyzing T Tauri stars, relatively little attention has been paid so far to obtaining a set of observational material which fully allows physical self-consistent modeling. In order to perform a complete analysis of the atmospheric structure of a T Tauri star, we were guided by the desire to cover the most important lines of Ca II (i.e., Ca II K 3933, Ca II H 3964, and the infrared triplet at 8494, 8542, and 8580 Å), of hydrogen, and of Na I, together with photospheric lines of all strengths. This requires full spectral coverage from at least 3900 to 8700 Å. Furthermore since these stars are known to vary on time scales from a few minutes up, it is very desirable to obtain all this data at essentially the same time.

The full astrophysical potential of any modeling of stellar activity can only be realized if based on resolved flux calibrated, and high S/N spectra obtained for many diagnostics at the same time. However, with most spectrographs the simultaneous demands of extreme spectral resolution and accurate spectrophotometry mutually exclude each other since the slit size affects both quantities in opposite ways. For this reason we elected to pursue a different approach, namely to use a high- and a low-resolution spectrograph concurrently.

The observations were carried out on 1985 May 19–21 with both the 3.6 m and 1.5 m telescopes of the European Southern Observatory on La Silla, Chile. The former telescope was used with its Cassegrain echelle spectrograph (CASPEC) and a RCA-CCD. With a slit size of 3″ × 3″ this instrument provided a spectral resolution of about $R = 12{,}000$. The spectrophotometric observations were performed concurrently on the 1.5 m ESO reflector on which an image dissector scanner was mounted. An entrance aperture of 8″ × 8″ resulted in virtually no light losses at the slit. Since this spectrograph was used in both its first-order (5350–8700 Å) and second-order (3700–5400 Å) configuration, a resolution of $R = 500$ or 1000 resulted. With CASPEC, four echelle frames were necessary to cover the same wavelength interval (with a gap from about 6700–7700 Å). The spectrophotometric observations were done simultaneously with CASPEC as much as possible, since T Tauri stars are expected to show irregular temporal variations, on top of which a rotational modulation may be imposed (see, for example, Bouvier and Bertout 1986*a*). All observations of a given star were typically obtained within 6 hr

TABLE 1

MODERATELY ACTIVE T TAURI STARS COVERED BY THE PROGRAM

Star[a] (1)	α (1950) (2)	δ (1950) (3)	Association[b] (4)	Sp[c] (5)	d[d] (6)	m_v[e] (7)
Sz 19 = CoD −76°486	$11^h05^m57^s5$	−77°21′50″	Chamaeleon 1	G2	170	10.6
Sz 68 = CoD −33°10685	15 42 01.4	−34 08 08	Lupus 1	K2	125	10.5
Sz 06 = LHα 332−20	10 57 50.8	−76 45 33	Chamaeleon 1	K2	170	11.2
Sz 65	15 36 16.3	−34 36 34	Lupus 1	K7–M0	125	12.2
Sz 98	16 05 01.0	−38 56 51	Lupus 3	K7–M0	125	12.4
Sz 82 = Th 12	15 52 51.1	−37 47 24	Lupus 2	M0	125	12.2
Sz 77	15 48 32.4	−35 47 47	Lupus 1	M0	125	12.5

[a] Star designation; Schwartz 1977.
[b] Associated dark cloud.
[c] Photospheric spectral type.
[d] Distance to the association, taken from Henize 1963 for the Chamaeleon and from Appenzeller *et al.* for the Lupus cloud complex.
[e] Visual magnitude, according to Appenzeller *et al.* 1983.

TABLE 2

LINE STRENGTHS

Star[a] (1)	W_λ(Hα)[b] (2)	W_λ(Hβ)[b] (3)	W_λ(He I)[c] (4)	W_λ(Li I)[c] (5)	F_λ(Hα)[d] (6)	F_λ(Hβ)[d] (7)	F_λ(K)[e] (8)	F_λ(H)[e] (9)	F_λ(8498)[e] (10)	F_λ(8542)[e] (11)	F_λ(8580)[e] (12)
Sz 19.....	−17.5	−2.4	−0.04	0.23:	1.78e8	4.20e7	3.37e7	2.68e7	3.41e6	8.96e6	5.48e6
Sz 68.....	−6.8	0.1	...	0.42	3.71e7	...	1.13e7	9.83e6	6.08e6	7.80e6	6.29e6
Sz 06.....	−34.8	−3.7	...	0.43	1.74e8	2.62e7	1.90e7	1.49e7	7.96e6	7.53e6	6.91e6
Sz 65.....	−3.3	0.5	−0.79	0.61	7.53e6	...	3.36e6	3.98e6	1.49e6	2.67e6	2.18e6
Sz 98.....	−19.6	−3.3	−0.16	0.51	5.96e7	1.26e7	1.56e7	7.06e6	6.03e6	1.20e7	6.38e6
Sz 82.....	−6.6	−2.2	−0.19	0.57	1.71e7	4.55e6	4.99e6	4.51e6	5.43e6	6.80e6	5.91e6
Sz 77.....	−17.4	−2.9	−0.21	0.60	5.22e7	7.06e6	6.97e6	6.75e6	5.42e6	7.27e6	6.72e6

[a] Star designation; Schwartz 1977.

[b] Equivalent widths of Hα and Hβ. The values shown represent the residual line strength after subtraction of the underlying photospheric absorption line strength, as measured from a corresponding standard star.

[c] Equivalent widths of He I 5876 and Li I 6707.

[d] Surface fluxes for Hα and Hβ. The values were obtained by using the distances, radii, and visual extinctions (assuming $R = 3.2$) from Tables 1 and 4. The lines represent the residual line strength after subtraction of the respective photospheric component.

[e] Surface fluxes for all major lines of Ca II. The flux of Ca II H does not contain the contribution from Hε. Except for H and K, the fluxes are corrected for an underlying photospheric contribution.

of each other. A final total of 602 echelle orders of the seven T Tauri stars from Table 1 and 560 orders of six spectrographic standards was obtained in three nights. The standard stars were Kopff 27 (A3 V), HD 196800 (G2 V), HD 188887 (K2 IV), BD -12°4935 (K7 V), HD 202560 (M0 V), and HD 200914 (M0.5 III).

The availability of the high-accuracy, separate fluxes for the T Tauri stars from the IDS greatly facilitated the photometric calibration of the echelle data. In addition, we were relieved of the need to observe photometric flux standards with the bigger telescope and could thus spend more integration time on our target stars. The details on how this external calibration was performed are already published (Finkenzeller and Basri 1985) and will not be repeated here. Since only a single entrance aperture was used with the echelle spectrograph, we cannot exclude the possibility that the high-resolution spectrograms contain a weak background or night sky contribution. However, since the observations were done in moonless nights the effect should be extremely small and only show up in strong emission features such as [O I]. The relative strength of the contamination of this stellar line can also be estimated by the strength of the pure night sky line from [O I] at 5577 Å. The final absolute accuracy of the photometric data is estimated (by evaluating different exposures of the same target, reduced with different flux standards) to be on the order of 4%–6% over the whole range, with relative errors within short wavelength intervals even smaller.

The reduced data are displayed in Figure 1 (low resolution) and Figure 2 (high resolution). In Figure 1 a G2 and M0 dwarf star from Jacoby, Hunter, and Christian (1984) are given for comparison purposes. The reference objects in Figure 2 were obtained with CASPEC. Since the standards were about 3 mag brighter than the T Tauri stars, no attempt was made to observe them with the IDS. The flux level for the standard stars at high resolution was adjusted by using the same external calibration technique as mentioned above, but with reference to objects with similar spectral type from the Jacoby, Hunter, and Christian (1984) catalog.

For wavelengths longer than 5700 Å, the high-resolution spectrograms have also been normalized to a flat continuum level in order to compare the material most easily. Due to the presence of numerous photospheric absorption lines, the true continuum level is increasingly difficult to establish shortward of about 5000 Å. In this region actual flux values are given. The high-resolution spectrograms are consistently sampled on a 0.15 Å grid which matches the actual resolution in the UV quite well but oversamples the signal in the IR. Due to the wide wavelength interval covered it is difficult to assign global S/N estimates. With the exception of the very ultraviolet and red, a S/N of at least 50 is present for most objects. The spectrograms given in Figures 1 and 2 were corrected for circumstellar/interstellar absorption as described below.

III. DETERMINATION OF STELLAR PARAMETERS

a) *Effective Temperatures*

For the determination of spectral types, the low-resolution IDS spectrograms were evaluated. Since we focused on obtaining high S/N, accurately calibrated spectra of our target stars rather than acquiring an extensive set of MK spectral standards, the library of stellar spectra of Jacoby, Hunter, and Christian (1984) was used for spectral classification purposes. The spectral type from Appenzeller, Jankovics, and Krautter (1983) could be verified to ±two subclasses. The main source of error is due to a peculiarity inherent with T Tauri stars: the filling-in of the deep absorption lines which also form the main spectral indicators. It is this particular effect which allows us to investigate the perturbed temperature structure in the stellar atmosphere. At this point, however, the systematic difference in the photospheric spectrum can slightly alter the adopted spectral type and lead to an uncertainty of up to two subclasses. It turned out that this uncertainty is of minor concern for the effects studied below.

No effort was made to provide an accurate estimate of the luminosity class, since the placement in the Hertzsprung-Russell diagram relies on the determination of the stellar luminosity, which can be done in a more rigorous way (see § IIIc). Absolute effective temperatures were assigned by using the temperature scale for young stars from Cohen and Kuhi's (1979) Table 7. All targets show the line of Li I 6707 in absorption (see Table 2), as should be the case for T Tauri stars. This line is discussed further in § IV*d*.

b) *Dereddening*

The determination of the amount of interstellar and circumstellar reddening of T Tauri stars is a difficult and controver-

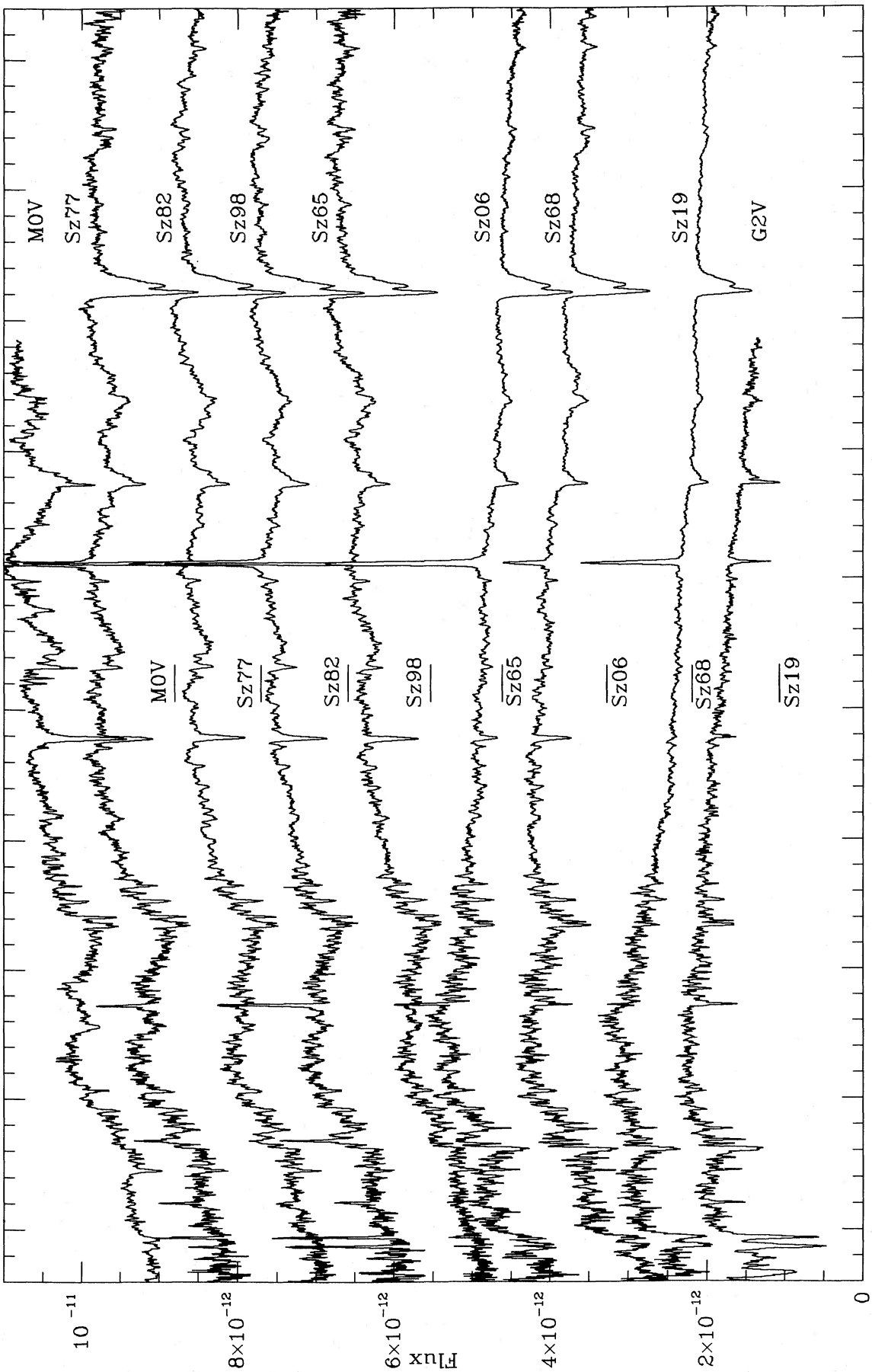

FIG. 1.—Dereddened Image Dissector Scanner tracings of seven low to intermediately active T Tauri stars. For each object, a first-order and second-order spectrogram were obtained. The two independent scans were merged at 5400 Å. For reference, a M0 V (*top*) and G2 V standard (*bottom*) from Jacoby *et al.* (1984) are also shown. With the exception of Sz 19, all T Tauri stars come in pairs consisting of a low and moderately active one. In order to read fluxes F_λ (ergs cm^{-2} Å^{-1} s^{-1}) from this diagram, for each star has a bias factor A and a scaling factor B has to be taken into account: $F_\lambda = B(F - A)$, where F is the plotted ordinate value. For the stars from bottom to top, A and B are (1) G2 V, 0, 1; (2) Sz 19, 1.1e−12, 1.136; (3) Sz 68, 2.2e−12, 0.682; (4) Sz 06, 3.3e−12, 0.364; (5) Sz 65, 4.65e−12, 0.0709; (6) Sz 98, 5.5e−12, 0.0455; (7) Sz 82, 6.6e−12, 0.0818; (8) Sz 77, 7.7e−12, 0.0455; and (9) M0 V, 8.8e−12, 0.909.

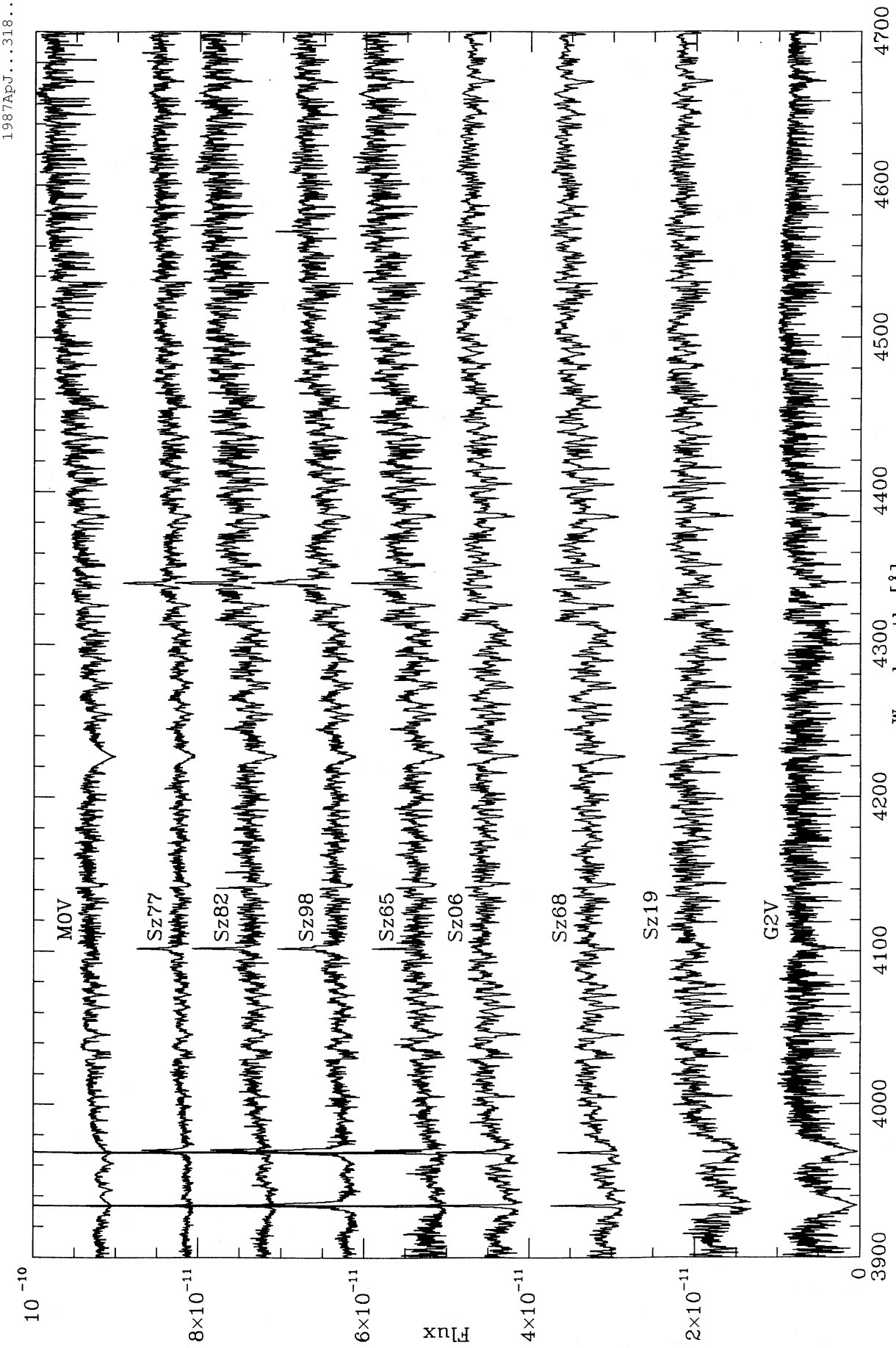

FIG. 2*a*.—High-resolution calibrated merged echelle spectrograms of the seven T Tauri stars from Fig. 1, ranging from 3900 to 4700 Å. Prominent emission lines are Ca II H and K, Hδ, and Hγ. As in Fig. 1, the stars *A*, and *B* are (1) G2 V, 0, 1; (2) Sz 19, 1.11e−12, 2.16; (3) Sz 68, 2.759e−12, 1.740; (4) Sz 06, 4e−12, 1; (5) Sz 65, 5e−12, 0.1; (6) Sz 98, 6e−12, 0.1; (7) Sz 82, 7e−12, 0.15; (8) Sz 77, 8e−12. 0.15; and (9) M0 V, 9e−12, 1.6.

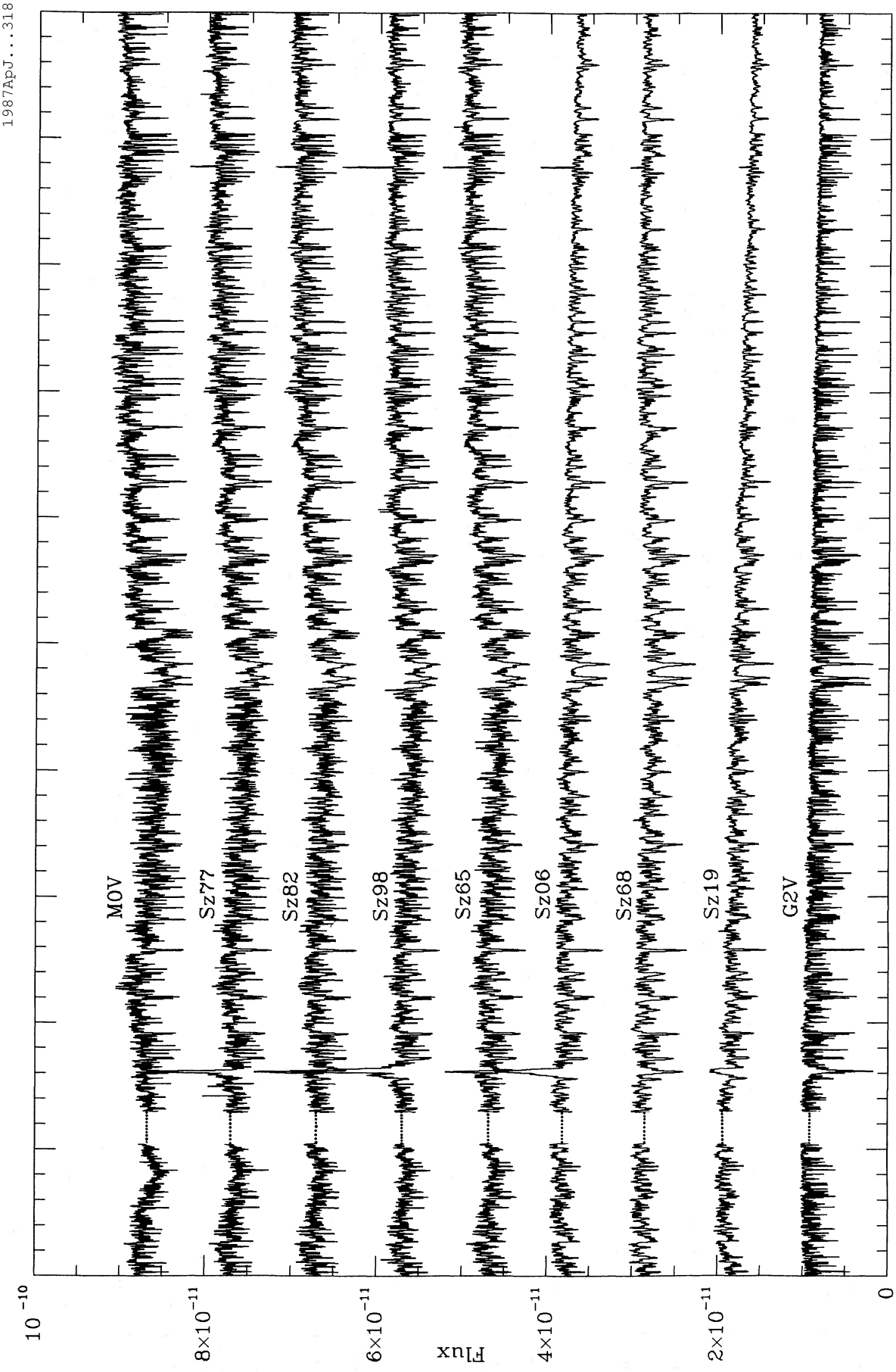

FIG. 2*b*.—Same as Fig. 2*a* but in the wavelength interval 4700–5700 Å. Due to a bad column in the CCD, the data from 4805 to 4830 Å are void. As in previous figures, the stars *A*, and *B*, are (1) G2 V, 0, 0.9; (2) Sz 19, 1e−11, 0.142; (3) Sz 68, 2e−11, 0.160; (4) Sz 06, 3e−12, 0.090; (5) Sz 65, 4e−11, 0.012; (6) Sz 98, 5e−11, 0.01; (7) Sz 82, 6e−11, 0.016; (8) Sz 77, 7e−11, 0.01; and (9) M0 V, 8e−11, 0.160.

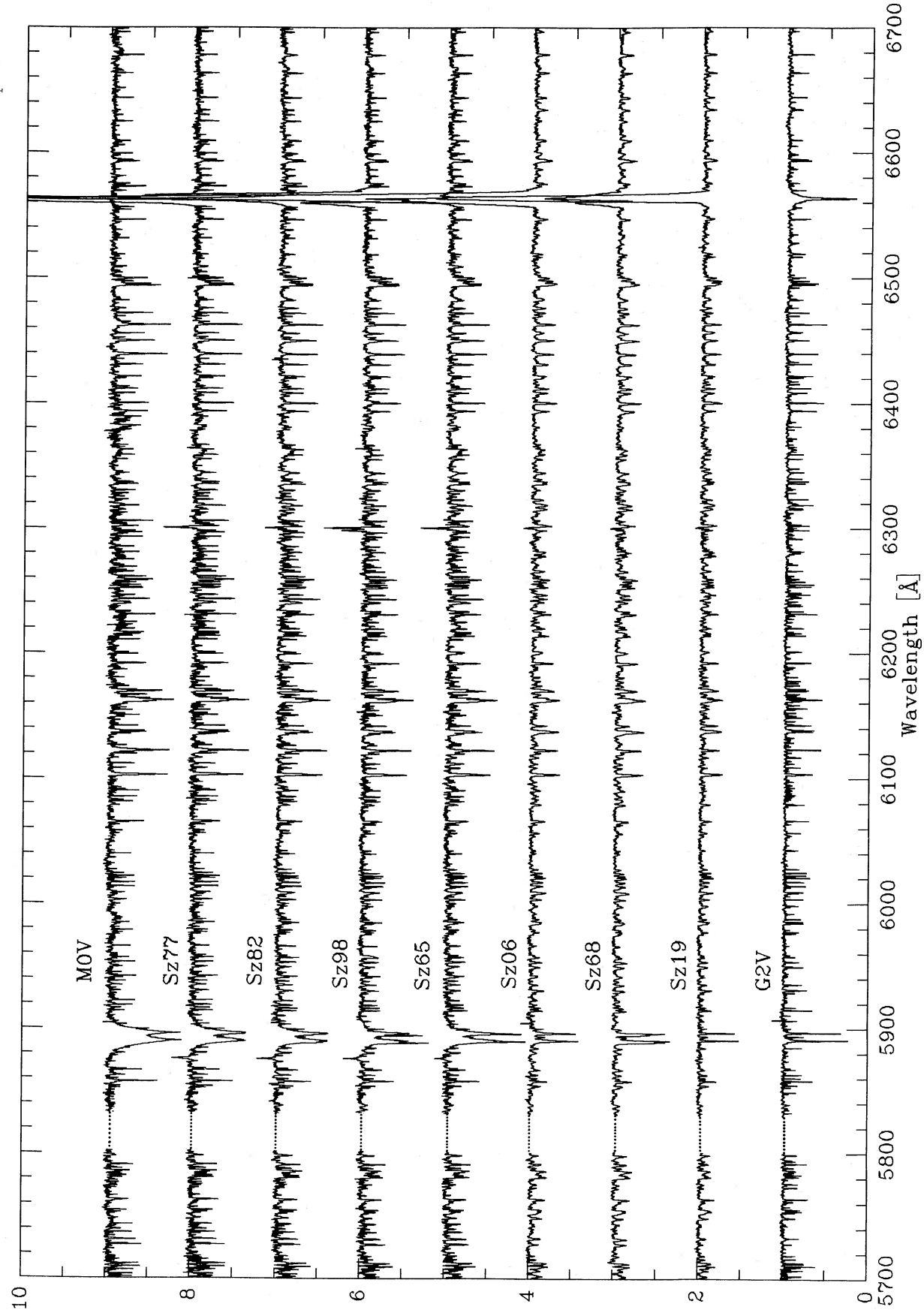

FIG. 2c.—In this and the following figure, the spectrograms were normalized to unity continuum level in order to compare them more easily, which due to line blending could not be done shortward of 5700 Å. The detector fault occurs here between 5800 and 5830 Å. The order of the stars is the same as in the previous figures. For flux values, the reader is referred to Fig. 1.

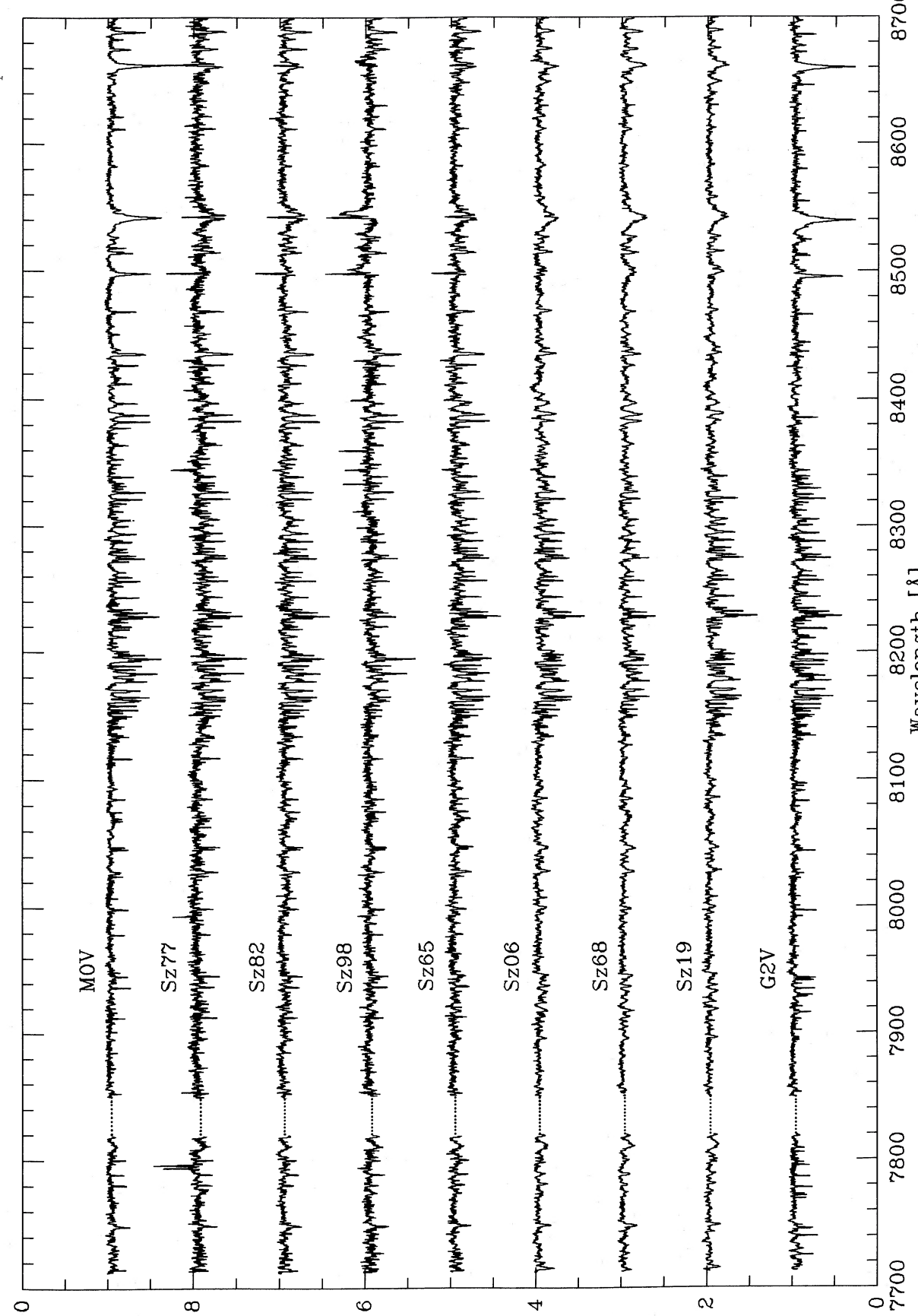

FIG. 2*d*.—Same as Fig. 2*c*, but in wavelength interval 7700–8700 Å. The Ca II triplet lines are the strong features at 8498, 8542, and 8552 Å. Void data are between 7820 and 7850 Å.

sial problem and affects all subsequent radiometric quantities in a direct way. An accurate derivation of A_v is thus a key problem of considerable importance. In particular, since T Tauri stars are known to possess circumstellar material which reprocesses visible stellar photons, reddening cannot be treated as though it arose only in the interstellar medium.

In order to deredden the T Tauri stars we have chosen a method of differential comparison with spectroscopic template stars for which accurate values of A_v are established. First, the standards from Jacoby, Hunter, and Christian (1984) were dereddened by using the quoted $E(B-V)$ and applying a standard reddening law (Savage and Mathis 1979) with $R = 3.1$. Then, the T Tauri stars were dereddened likewise. Since we had no *a priori* knowledge of the expected A_v value, a series of dereddened spectra was obtained for each object, incrementing A_v by 0.1 each time. After that, the ratio between the T Tauri and standard star was set up in the wavelength range 3700–7450 Å. The value of A_v was considered to be correct for the number giving a constant ratio between T Tauri and a standard star. In order to avoid systematic effects attributable to a possible contribution of UV veiling or excessive near-IR emission, the actual wavelength interval in which the comparison was made was restricted to the region between 4500 and 6500 Å. The A_v values derived in this way are listed in Table 4. Various cross-checks of the procedure described above lead to an error estimate of about ± 0.2 in A_v. The true external error is most likely larger, since we cannot rely on a standard reddening law with $R = 3.1$. Ideally, one would like to distinguish between foreground reddening (with $R = 3.1$, presumably), and reddening within the dust cloud in which the star is embedded (with, e.g., $R = 4.2$, as found by Herbst *et al.* 1982 for several R associations), but this is extremely difficult. A higher value of R would increase the true stellar flux in the visible and leave the infrared contribution basically unaltered.

An even more important systematic problem arises from the sensitivity of the results to the spectral standard employed. For example, it makes a significant difference whether one uses giants or dwarfs. A difference of two spectral subclasses can also be important. These effects are particularly apparent in spectral class K. Since T Tauri stars are really most like subgiants, it would be preferable to use subgiant spectral standards. In this work we have used the nearest available dwarf in the Jacoby *et al.* catalog. Since giants tend to be deficient in blue flux relative to dwarfs, this choice was made to minimize spurious detections of UV excess. In general, however, the value of reddening derived with giants is less than that from dwarfs. In the worst case we find differences of half a magnitude in the reddening derived from different plausible standards. Our view therefore is that the reddening values given here are really preliminary and upper limits, and an effort is underway to obtain flux distributions for a set of standard stars that will allow a more definitive determination of the reddening. We note that the effect of lowering the reddening is to decrease the *stellar* luminosities defined in the next section and therefore to increase the fraction of nonstellar luminosity apparent in several cases.

An independent justification of the magnitude of A_v can be gained by plotting linear polarization (at 5885 Å) versus the derived A_v values (Fig. 3), since for all the T Tauri stars polarization measurements from Bastien (1985) are available. A good correlation is found in the sense that objects having high readings of A_v show high polarization. This relation is free from any *a priori* assumptions. Since the objects are associated

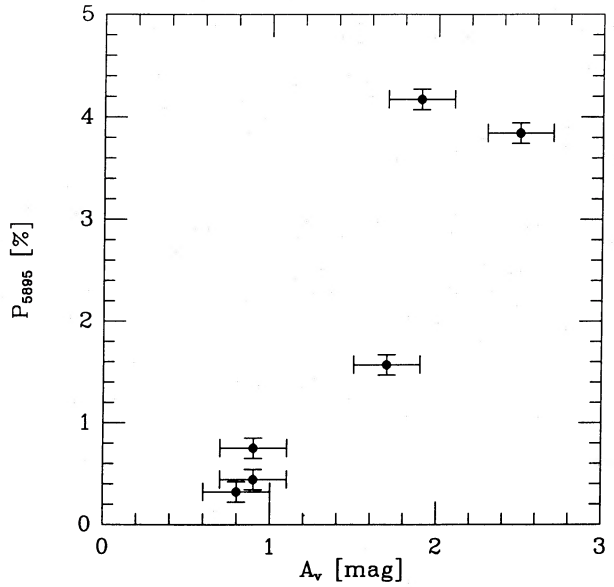

FIG. 3.—Linear polarization at 5885 Å (Bastien 1985) versus. A_v, derived differentially from standard stars. For more details, see text.

with different molecular clouds and probably embedded at different depths, the bias of about 0.8 mag in Figure 3 should not be attributed to a general foreground extinction. It is interesting to note that those stars which have the highest A_v values (Sz 19, Sz 68, and Sz 06) have fairly high $v \sin i$ values, too.

c) *Luminosities*

Apart from the usual uncertainties in the stellar data, one is faced with two additional problems when determining accurate luminosities of T Tauri stars: one has to apply large corrections (1) for wavelength intervals not observed (i.e., a bolometric correction for the infrared range where a considerable amount of energy can be radiated), and (2) for light removed by circumstellar and/or interstellar extinction.

The contribution to the stellar luminosity shortward of 3700 Å is negligible for cool stars and has not been taken into account here. However, since T Tauri stars radiate a considerable amount of their energy at infrared wavelengths, a correction for the flux longward of the last available IDS value at 8700 Å had to be made. For this purpose, we used published *HJKL* photometry (Appenzeller, Jankovics, and Östreicher 1984) and searched the *IRAS* data base. All the T Tauri stars were detected by *IRAS*. For the four *IRAS* fluxes conversion factors were kindly supplied by M. Cohen, taking into account overlapping between adjacent bands. Unobserved infrared flux beyond the last available data point was accounted for by extrapolation with a Planck function (see, e.g., Cohen 1973). By integrating the *non-dereddened* IDS spectrograms and over all available *HJKL* and *IRAS* data points a luminosity was obtained (see Table 3). This luminosity is referred to as "systemic" below since it is a measure of all contributions from the photosphere, an envelope, and possibly a disk or an unseen red companion star. In the case of spherical symmetry, this luminosity is a true lower limit of the systemic luminosity, since it assumes that no light is removed by interstellar dust, i.e., the light is only supposed to be redistributed from the optical to the IR by dust near the star.

The major drawback of this technique is that it does not take into account any foreground or intracloud reddening which

TABLE 3

NEAR-IR ENERGY DISTRIBUTION AND LUMINOSITIES

Star[a] (1)	J[b] (2)	H[b] (3)	K[b] (4)	L[b] (5)	L_{IRAS}[c] (6)	$L_{V\ and\ NIR}$[d] (7)	L_{obs}[e] (8)	L_{phot}[f] (9)
Sz 19.....	...	...	...	...	1.08	2.26	3.34	4.6
Sz 68.....	2.68e−13	1.91e−13	9.54e−14	3.35e−14	1.21	0.96	2.17	3.0
Sz 06.....	...	...	...	...	0.48	1.32	1.80	2.7
Sz 65.....	...	...	...	...	0.15	0.39	0.54	0.32
Sz 98.....	5.06e−14	4.10e−14	2.53e−14	1.17e−14	0.25	0.21	0.46	0.23
Sz 82.....	8.63e−14	6.26e−14	3.02e−14	8.12e−15	0.19	0.26	0.45	0.50
Sz 77.....	5.06e−14	3.67e−14	1.87e−14	5.77e−15	0.05	0.16	0.21	0.23

[a] Star designation; Schwartz 1977.
[b] Near-infrared fluxes, according to Appenzeller *et al.* 1983. *JHKL* magnitudes are given in ergs cm^{-2} s^{-1} Å^{-1}.
[c] Far-infrared luminosity longward of 12 μm, based on *IRAS* data. A correction for unobserved flux longward of 100 μm was added by a technique described by Cohen 1973.
[d] Observed visible and near-infrared luminosity, obtained by a trapezoidal integration of the IDS spectrogram and the *JHKL* photometry.
[e] Sum of cols. (6) and (7). This luminosity represents the *observed* luminosity, not corrected for interstellar/circumstellar reddening.
[f] Photospheric stellar luminosity, based on an extrapolation and integration of the dereddened IDS spectrogram.

may be substantial for objects which are embedded in molecular cloud complexes. In addition, for a discussion of the stellar photospheres alone one might not wish to use the "systemic" luminosity. Therefore, an alternate procedure which explicitly takes reddening into account was devised.

In order to obtain a luminosity characteristic of the stellar photosphere alone (referred to as "photospheric" luminosity below) we relied on the *dereddened* IDS spectrograms which we obtained as described above. Since no dereddened fluxes were available beyond 8700 Å from this data set, for the region beyond that point an extrapolation was made with a Planck function corresponding to the appropriate effective temperature of the star. The height of this function was normalized so as to smoothly extend the stellar flux. This is justified since the infrared *stellar* photospheric energy distribution can be approximated to a good degree by a blackbody law. The combination and integration of these purely "photospheric" contributions provided a stellar luminosity which we have chosen to be the basis of all further parameters directly related to the stellar atmosphere (Table 4). The luminosity provided in this way takes explicitly into account circumstellar and/or interstellar reddening and is also consistent with the other stellar parameters (cf. § III*d*). Of course, the result depends on the accuracy with which extinction and hence the absolute stellar energy distribution in the optical can be established. This approach is clearly more favorable for objects of moderate or low activity with unobscured photospheres than with extremely active stars. Mainly for this reason and the lack of suitably absolute calibrated data, the outlined procedure has not been used for T Tauri stars before.

A H-R diagram of the considered T Tauri stars is given in Figure 4. The dashed lines refer to the "systemic" total luminosities; solid lines are the "stellar," or photospheric luminosities. Apart from errors in the dereddening procedure, the differences between stellar and total luminosities yield information on the circumstellar environment. With Sz 19, Sz 68, and Sz 06 the observed luminosities are distinctly lower than the corrected stellar luminosities (see Table 3). This finding is also valid if the true value of R should be bigger than $R = 3.1$ (which was adopted here), since, e.g., $R = 4.2$ would raise the corrected stellar flux even further. We conclude that a considerable fraction of the stellar flux from these stars is lost before it can reach us. This finding is consistent with the suspicion that we see these systems nearly edge-on through a cir-

TABLE 4

STELLAR PARAMETERS

Star[a] (1)	P_{5885}[b] (2)	A_v[c] (3)	V_*[d] (4)	V_{MC}[e] (5)	$v \sin i$[f] (6)	P[g] (7)	$R/R_\odot$[g] (8)	$M/M_\odot$[h] (9)	log g[h] (10)	Age[h] (11)
Sz 19.....	3.84	2.50	5.7	...	33	4.3	2.8	1.80	3.80	4.0e6
Sz 68.....	1.57	1.7	1.8	4.7	41	3.3	2.65	1.60	3.80	2.8e6
Sz 06.....	4.17	1.9	3.5	...	32	4.0	2.65	1.55	3.82	3.0e6
Sz 65.....	0.44	0.9	10.2	4.4	21	3.3	1.35	0.65	3.99	3.0e6
Sz 98.....	0.32	0.8	5.0	...	<15	>3.4	1.00	0.60	4.22	7.0e6
Sz 82.....	...	0.8	3.0	...	<15	>4.7	1.40	0.65	3.96	2.5e6
Sz 77.....	0.75	0.9	1.0	4.4	<15	>3.4	1.00	0.60	4.22	7.0e6

[a] Star designation; Schwartz 1977.
[b] Percent linear polarization at 5885 Å, according to Bastien 1985.
[c] Visual extinction in mag, derived with respect to an unreddened standard star.
[d] Stellar systemic velocity in km s^{-1} in the LSR, derived by cross-correlating photospheric lines with those of standard stars.
[e] CO velocity of the associated dark cloud in km s^{-1} in the LSR, according to Murphy *et al.* 1986.
[f] $v \sin i$ in km s^{-1}, derived by evaluating the first zero of the power spectrum.
[g] Estimated rotational period, assuming that we view the star edge-on.
[h] Stellar radius, mass, log surface gravity, and age, as read off the H-R diagram given by Cohen and Kuhi 1979.

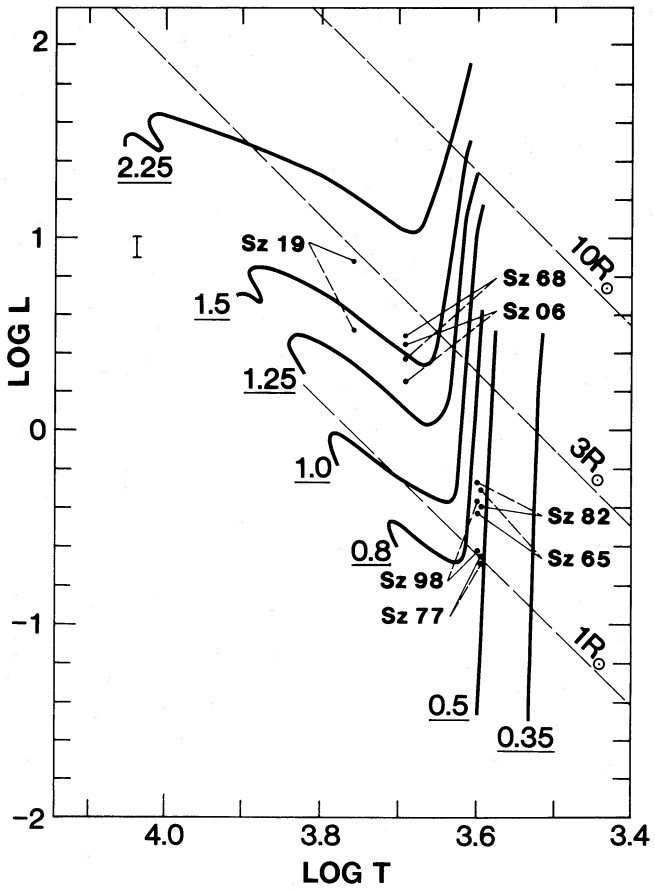

FIG. 4.—The H-R diagram for the seven T Tauri stars, with convective-radiative evolutionary tracks, and lines of constant stellar radius from Cohen and Kuhi (1979). The error bar at the left margin corresponds to the uncertainty of a photospheric luminosity due to ± 0.2 magnitudes in A_v. The values referenced by a dashed line are the systemic bolometric luminosities as derived by integrating the observed flux, the solid line points to a photospheric luminosity. For the determination of the stellar parameters R, M, and g, these photospheric luminosities were used.

cumstellar disk which scatters photons out of the line of sight rather than absorbing and reemitting it in the IR. This view is also supported by the fact that these systems have only weak interstellar sodium absorption components, although their A_v values are on the order of 2.

Other objects in our sample show a smaller difference between the two types of luminosities or even have an observed luminosity which is higher than one would expect from a photosphere alone. The situation for Sz 82 and Sz 77 can be easily explained by complete reprocessing of stellar photons and negligible interstellar extinction. All visible stellar radiation which is removed from the beam is reradiated at infrared wavelengths, suggesting a very small foreground extinction. Since Sz 77 is located in the Lupus 1 dark cloud, other objects in this association (Sz 65 and Sz 68) are likely to possess the same small foreground extinction of about 0.9 mag. For Sz 65 and Sz 98 the interpretation of the two sets of luminosities is more complex since their observed total energy distribution is higher than what would be expected from a dereddened single photosphere. Further peculiarities of Sz 98 are discussed in more detail below. It cannot be ruled out that additional energy sources (IR companion, self-luminous disk) are contributing flux in these systems.

d) Radii and Gravities

Placing the objects in an H-R diagram with evolutionary tracks (e.g., from Cohen and Kuhi 1979) allows a determination of masses, radii, and ages. It is straightforward from these quantities to compute surface gravities. These parameters are given in Table 3. The luminosity obtained from the dereddened photospheric energy distribution was used in order to establish these values. Any initial errors in L, together with uncertainties in $T_{\rm eff}$ and systematic errors inherent in the evolutionary tracks are directly translated to the derived quantities. In particular, the estimates of the radii are accurate to about ± 0.15, and the masses to ± 0.05 solar units. Together with the initial uncertainty in L this leads to an error of about 18% in surface gravity, corresponding to 0.09 dex. In this context, it is gratifying to note that "photospheric" surface fluxes $F_L = L_{\rm ph}/4\pi R_*^2$, computed by using the "photospheric" luminosities and the stellar radii, are typically within 10% of the corresponding $\sigma T_{\rm eff}^4$ values. This agreement can be taken as a further justification for the methodoligocal approach chosen and the accuracy of all parameters involved.

e) Rotational Velocities

An accurate determination of $v \sin i$ is crucial for any quantitative work on line profiles and an important quantity related to stellar activity. Three techniques (direct matching, autocorrelation and Fourier transforms) were applied to recover values for $v \sin i$; all of them showed consistent results. In the first approach a comparison between a given wavelength interval of a T Tauri star and a corresponding standard star was made. The spectrogram of the initially nonrotating standard was convolved with a rotational function taken from Gray (1976). This artificially created set of rotational standards was overlaid onto the target stars. For our material the accuracy is about ± 4 km s^{-1} with this technique.

Another method is to set up the autocorrelation function for each object and to calibrate the width of the autocorrelation peak (see Hartmann *et al.* 1985 for more details). We have applied this method, too. The main error source is caused by the determination of the baseline of the autocorrelation function for stars with different $v \sin i$. Also, line blending can affect the FWHM of the autocorrelation peak. An internal error of about ± 6 km s^{-1} is inherent in this technique for our data.

The most accurate treatment in order to determine $v \sin i$ is to evaluate power spectra of line profiles since in this approach no *a priori* assumptions are made. The available sampling step and S/N allows the detection of the characteristic zeros in the power spectra down to a lower limit of 14 km s^{-1}. In order to reduce what is referred to as "beating" we have chosen to chop longer spectra into smaller segments and average the power spectra of these. Segment lengths of 512 or 256 pixels gave good results, averaging over typically eight or 16 individual segments. The errors with this technique are ± 2 km s^{-1}, and the results agree well with the ones from the other approaches. An independent external check can be made by comparing the estimate from Bouvier *et al.* (1986) of $v \sin i$ for Sz 19, Sz 68, and Sz 06 of 30 ± 5, 48 ± 7, and 35 ± 5 km s^{-1} with 33, 41, and 32 ± 2 km s^{-1} derived in this work. The values of $v \sin i$ given in Table 4 are from the power spectra analysis. Together with the radii determined above the range of values of the rotational period can be guessed, assuming that we see the system edge-on. These are all on the order of a few days to a week.

In Table 4 a trend of the dependence of rotational velocity with spectral type is present in the sense that the cooler the star, the smaller $v \sin i$. This trend is in agreement with Hartmann *et al.*'s (1986) data which is on a statistically more sound basis. Their finding that 30% of all T Tauri stars in Taurus/Auriga and Orion rotate faster than $v \sin i = 15$ km s^{-1} compares nicely with what we found in our much smaller sample where three out of seven objects show this behavior. In particular, these three objects (Sz 19, Sz 06, and Sz 68) are systems which are definitely not viewed pole-on, a finding which will help in the interpretation of their envelope characteristics.

f) *Radial Velocities*

Systemic radial velocities were obtained for all target stars by cross-correlating the spectrograms with standard stars and evaluating the position of the correlation peak. The velocities of the standards were taken from Abt and Biggs (1972) and the *Bright Star Catalog*. A correction for the solar motion was applied in order to convert the heliocentric velocities to the LSR frame of rest. All velocities presented in this work are in the LSR. By mutually cross-calibrating the standards with each other, the internal error could be estimated to be on the order of 1 km s^{-1}. The external error is dominated by the uncertainty of the velocities of the standards which is about 2 km s^{-1}. The photospheric radial velocities are given in Table 4.

For Sz 68 Herbig (1977) cites a systemic velocity of -6 km s^{-1}, compared to $+1.8$ km s^{-1} obtained here. It should be kept in mind that our data quality is superior to his, and that the CO velocity of the associated molecular cloud of $+4.7$ km s^{-1} agrees much better with our higher value. A comparison with radio data for the other associations (kindly made available to us by R. Cohen prior to publication) indicates no systematic differences between systemic and molecular cloud velocities within the error margins. On the basis of this material, we can almost rule out the possibility of close, massive companions. The chosen T Tauri stars are most likely not members of double star systems.

IV. LINE PROFILES AND STRENGTHS

The spectrograms displayed in Figures 1 and 2 can give only an overall impression of the appearance of a particular object. For a more refined look at profile shapes selected lines are presented in Figure 5. We have chosen to display Ca II K and Hβ which are inner atmosphere diagnostics, Hα to probe a region further out, and the two sodium lines as a tracer of the interstellar/circumstellar medium. All frames are centered at the appropriate line center and are ± 500 km s^{-1} wide so that velocity structures can be compared easily. In order to recover a velocity for a particular feature, one may add the corresponding number of pixels, multiplied by a scaling factor given in the figure legend. This will be relative to the systemic velocity which is indicated by the vertical line. Kinematical measurements related to Figure 5 are given in Table 5.

a) *Balmer Lines*

The Hα and Hβ line profiles of the stars observed show a wide range of strength and structure. From Table 2 it can be seen that the Hα equivalent widths range from -3.3 to almost -35 Å. For the determination of these values, the contribution of an undisturbed photosphere has been subtracted. As pointed out above, the targets were selected in a way to yield both a weak and an intermediately active T Tauri star as referenced by its Hα line strength. (For comparison, the most active main-sequence dwarf stars have Hα equivalent widths of about -0.1 Å.)

For five of the stars Balmer decrements can be computed from Table 2. The ratio of the Hα versus Hβ *surface fluxes* yields values between about 4 and 7, without an obvious dependence on $T_{\rm eff}$. The magnitude of the decrement is not related to the Ca II surface flux either. The selected objects display various degrees of chromospheric activity as indicated by the order of magnitude spread in the K-line surface fluxes. That the Balmer decrement is much more constant arises from the fact that the Balmer lines are fairly well correlated with the K-line (see § IV*d*). It is interesting to note that a discussion of Balmer *equivalent width* decrements is less meaningful, as then the envelope line is normalized to the continuum of the associated star. The varying contrast between continua of different strength and the investigated line introduce effects without physical significance. It is this effect which is primarily responsible for the small Hβ equivalent widths measured for Sz 68 and Sz 65 in Table 2 (see also § IV*c*).

The line profiles of Ca II K, Hα and Hβ, and NaD$_{1,2}$ are given in Figure 5. Ca II K is discussed in § IV*b*. The latter three lines originate partially in the circumstellar environment and can provide information about macroscopic flow patterns in the envelope of the star. Evidence of either a red absorption component or a steep red line wing in the Balmer line profiles can be unambiguously seen in Sz 65, Sz 98, Sz 82, and Sz 77. A

TABLE 5

KINEMATICAL DATA OF LINE PROFILES

Star[a] (1)	$v_{\rm He\,I}$[b] (2)	$v_{\rm [O\,I]}$[c] (3)	$v_{\rm em}$[d] (4)	$v_{\rm abs}$[d] (5)	$v_{\rm blue}/v_{\rm red}$[d] (6)	Ratio[d] (7)	$v_{\rm em}$[e] (8)	$v_{\rm abs}$[e] (9)	$v_{\rm blue}$[e] (10)	$v_{\rm red}$[e] (11)	Ratio[e] (12)
Sz 19.....	...	−1	−1	...	−170/260	0.7	13	...	−130	130	1.0
Sz 68.....	...	13	−117, 45	−51	−300/300	1.0	18	...	−170	170	1.0
Sz 06.....	...	2	3	...	−310/310	1.0	3	...	−170	170	1.0
Sz 65.....	12	12	7	−32, 71	−210/280	0.7	15	...	−140	170	0.8
Sz 98.....	20	18, −80	−143, 17, 123	−92, 105	−300/300	1.0	00	−84, 39	−300	300	1.0
Sz 82.....	3	10 (n.s.)	−21	...	210/130	1.6	−8	...	−130	130	1.0
Sz 77.....	18	9 (n.s.)	−8	...	−300/200	1.5	12	...	−110	110	1.0

[a] Star designation; Schwartz 1977.
[b] Velocity of the He I 5876 emission line. All velocities are in km s^{-1} and refer to the LSR.
[c] Velocity of the stellar [O I] 6300 emission line.
[d] For Hα the velocities of the local emission maxima, local absorption minima, maximum blueward/maximum redward extend at continuum level, and the ratio of the latter two numbers are given.
[e] Same as above, but for Ca II K.

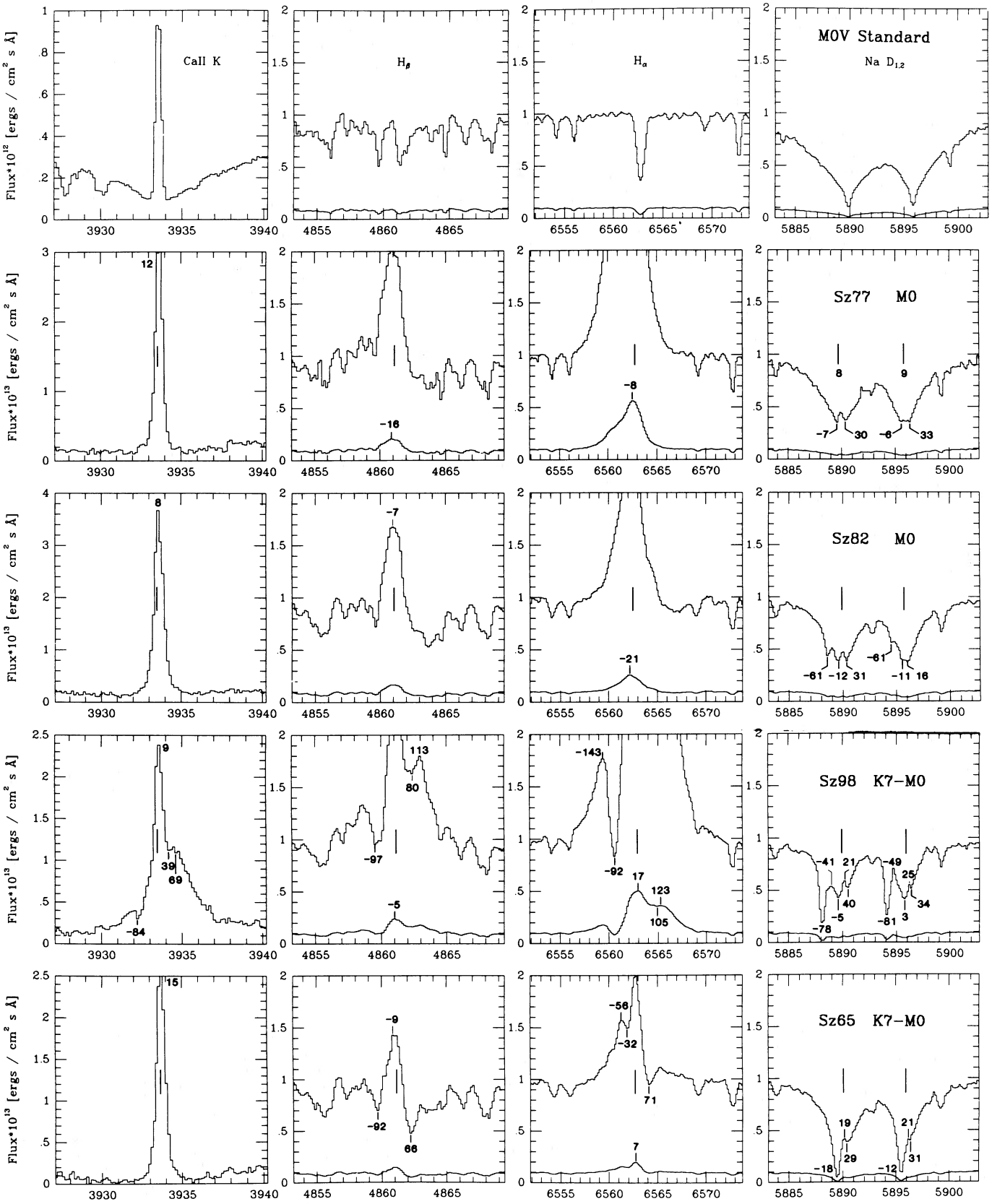

FIG. 5.—Selected line profiles at an expanded scale for each T Tauri star from Figs. 2*a*–2*e*. From left to right, each series consists of the lines of Ca II K, Hβ, Hα, and NaD. Except for Ca II K, all plots are normalized to continuum level and cover ±500 km s^{-1} from the center. One pixel corresponds to 11.4, 9.3, 6.9, 7.5 km s^{-1}, respectively. For each object, the systemic velocity from Table 4 is indicated by a vertical bar. All velocities are in the local standard of rest.

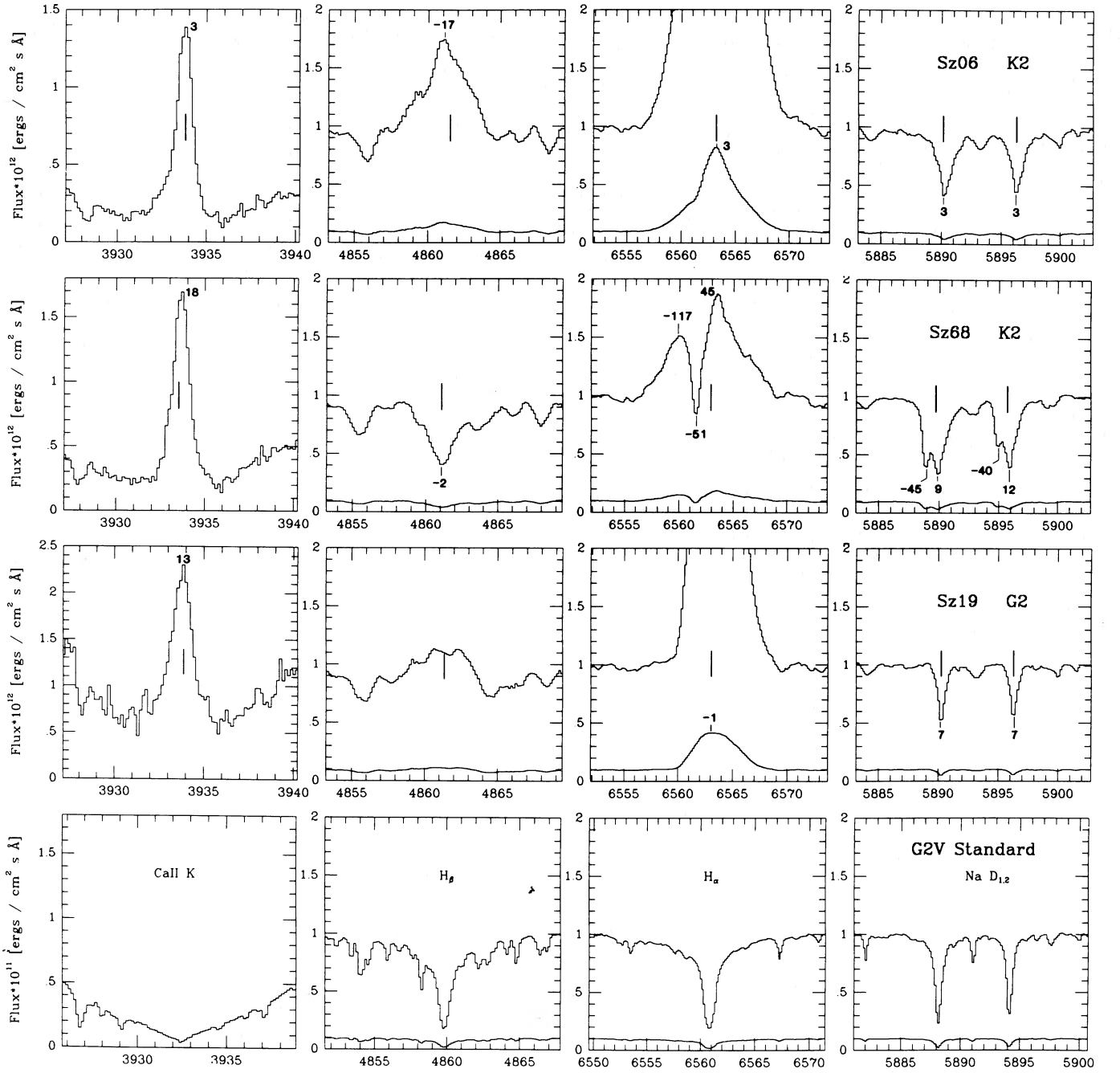

FIG. 5.—*Continued*

comparison with the corresponding sodium line profiles shows that in all these cases an absorption structure seems to be present in the red NaD wing as well. These features are enhanced when standard spectra are divided out (reducing confusion due to the photospheric component) as demonstrated by Finkenzeller and Basri (1986).

A blue Balmer absorption component or a steep blue wing is characteristic of Sz 06, Sz 68, Sz 65, and Sz 98. With the possible exception of Sz 06, a blueshifted NaD absorption component can be verified for these objects. Blueward displaced sodium components are also present for Sz 77 and Sz 82, although a corresponding feature in the hydrogen lines is less obvious for these stars. Two objects (Sz 65 and Sz 98) show evidence of both redward and blueward absorption components in the Balmer and sodium lines. One object (Sz 19) displays symmetric Balmer lines with no absorption components and narrow symmetric sodium lines. The sodium lines of Sz 19 are filled in by an unshifted emission component on which a centered circumstellar/interstellar absorption feature is superposed. This can be seen in the appropriate difference plot (Finkenzeller and Basri 1985, their Fig. 2*b*).

The possible presence of interstellar absorption components could complicate a simple interpretation of the sodium lines, but on the basis of typical line strengths (a few mÅ) and posi-

tions (a few km s^{-1}) of typical interstellar absorption lines, they should not affect our conclusions. No interstellar Ca II absorption components are present in any of the objects (Fig. 5). It is less clear whether the apparent absorption features in the sodium lines are due to a circumstellar *absorption* component shifted in wavelength, or are the consequence of an *emission* component of chromospheric origin. Analysis of various other photospheric lines of T Tauri stars in § V shows that under certain conditions the flux at line center can indeed be enhanced, as does the theoretical analysis of Cram (1979). On the other hand, the qualitative comparison of the sodium line profiles between the T Tauri stars and standard stars of similar spectral type do not suggest an enhanced line core. Except for the M stars, the ratio plots yield no narrow emission features as in the weaker photospheric lines. Furthermore, the absorption features do not straddle line center as would be expected for minima of a surface emission feature. The final resolution of this issue awaits explicit calculation of the sodium lines in a realistic stellar chromospheres model.

Until now, the presence of inverse P Cyg profiles in T Tauri stars was known to occur only with the most active examples. Three of the low-activity objects presented here are only marginally reddened ($A_v \leq 0.9$ mag) but show this phenomenon. This suggests that the formation of inverse P Cyg–type line profiles is not directly related to the presence of infalling material with high column densities. The combination of radiation transport effects with nonspherical geometries as proposed by various authors (e.g., Ulrich and Knapp 1985) may be a more acceptable scenario. It is very important to determine whether the redshifted components are diagnostic of continuing accretion in these objects, which have rather mild circumstellar envelopes compared to the "classical" T Tauri stars. The presence of such a variety of profile behavior in objects of this type is fortunate. The intrinsic stellar spectrum can be understood and removed much more easily since it is visible through the circumstellar material, whereas that is less the case in most of the young stars studied so far.

b) Ca II *Lines*

Together with the line of neutral calcium at 4226 Å and the infrared triplet lines of singly ionized calcium, the lines of Ca II H and K in the UV form a complete set of the astrophysically most important transitions in this element. We have resolved flux-calibrated line profiles for these lines, although for the fainter objects in the UV only the emission components and not the photospheric line wings were exposed properly. The surface fluxes given in Table 2 for Ca II H and K are the total fluxes, including any remaining continuum at the photospheric line center. The Ca II H readings are corrected for the contribution from Hε. For the IR triplet lines, the stellar photospheric contribution has been subtracted.

As a general rule, much less profile structure can be seen in Ca II than in hydrogen. There are several cases in which Hα and Na D show pronounced absorption components whereas Ca II K does not. This finding cannot be attributed only to the difference in resolution on the velocity scale, which can account only for a factor of 1.5 (6.9 km s^{-1} $pixel^{-1}$ at Hα, 11.4 km s^{-1} $pixel^{-1}$ at Ca II K). Clearly, the fact that the formation of this line is different than for hydrogen is reflected in the different profile. With the exception of Sz 98 (which is peculiar on several counts) no circumstellar or interstellar contributions are present in calcium. Previous work (Calvet, Basri, and Kuhi 1984) shows that for hydrogen a geometrically extended shell has to be assumed in order to explain the line profiles observed in a "typical" T Tauri star. A line formed close to the surface of the star, as predicted for chromospheric Ca II, is expected to be relatively narrow and symmetric. We conclude from the appearance of the profiles that chromospheric components of H and K are present in all the stars; Sz 98 has an obvious envelope contribution as well. An independent argument that Sz 98 has an extended (optically thin) envelope is also its (Ca II K)/(Ca II H) ratio of 0.5. It should be expected that as one examines stars with even stronger Hα lines, the envelope contribution to H and K will become more dominant. Only with high-resolution profiles can the two rather different phenomena be easily separated.

A quantity which can be used to constrain the region where lines are formed is the ratio V_r/V_b, i.e., the ratio of maximum extent of emission in the red and blue, at continuum level. Since for an exact determination of this value the spectrograms have to be well exposed at continuum level, only little material has been analyzed so far. This method was first employed by Kuan and Kuhi (1975) for objects with extended envelopes. In our case we have evidence from semiempirical models (Calvet, Basri, and Kuhi 1984) that the line formation region of Ca II is of chromospheric origin and must be close to the stellar surface. In Table 5 we give the ratio V_r/V_b for Hα and Ca II K. It is obvious that Ca II displays values much closer to 1.0. If a velocity field at the site of formation of Ca II K (i.e., close to the star) were present, this would result in a corresponding line asymmetry which we do *not* observe. This finding indicates that close to the star in the chromosphere no velocity field is present. Calcium has a smaller velocity width than hydrogen at its base. The hydrogen lines have a contribution from further out in the envelope with the additional problem of more complicated radiation transport effects, so are less straightforward to interpret. To summarize the observational material for easy reference, the main characteristics for each target object are given in Table 6.

c) *The Lines of* He I *and* [O I]

For four of seven objects, the line He I 5876 shows up in emission; the corresponding equivalent widths are given in Table 2. There is a clear trend that in our sample the line strength increases toward cooler temperatures and is independent of the Hα emission flux. Compared with the relation found by Cohen and Kuhi (1979) (their Fig. 14, indicating a proportionality for an Hα equivalent width larger than about 20 Å), our data probe much less active objects. In addition, the smallest equivalent width we can reliably measure is on the order of 0.02 Å, whereas theirs is 0.5 Å. The appearance of this line for the cooler stars is largely a contrast effect; the earlier type stars are more than a factor of 10 more luminous than the cooler ones. If the intrinsic He I luminosity (related to the presence of hot material $T > 10^5$) is approximately the same in all the stars, one expects He I emission at the level visible in the cool stars to be masked by hotter photospheres.

Another prominent emission lind apparent from Figure 2 is [O I] 6300.26 Å. This transition originates in a tenuous region and probes regions further away from the star. We do not give surface fluxes because this line is from a geometrically very extended regions. [O I] has the disadvantage of being polluted by a contribution of the night sky which could not be corrected for in our high-resolution spectograms. Due to the night sky contribution, accurate line strengths could not be given. On the other hand, it is quantitatively clear that [O I] does not

TABLE 6

MORPHOLOGICAL CHARACTERIZATION OF THE PROGRAM STARS

			Position of Absorption Components		
Star[a] (1)	Activity[b] (2)	$v \sin i$[c] (3)	NaD[d] (4)	Hα[e] (5)	IR Excess[f] (6)
Sz 19.....	intermediate	fast	centered	centered	intermediate
Sz 68.....	weak	fast	blue	blue	intermediate
Sz 06.....	high	fast	...	blue	intermediate
Sz 65.....	weak	moderate	blue, red	blue, red	large
Sz 98.....	intermediate	slow	blue, red	blue, red	large
Sz 82.....	weak	slow	blue, red	red	small
Sz 77.....	intermediate	slow	blue, red	red	small

[a] Star designation; Schwartz 1977.
[b] Relative degree of stellar activity, as judged from the Ca II K and Hα emission-line strength.
[c] Relative apparent rotational velocity.
[d] Relative position of additional absorption components of $NaD_{1,2}$.
[e] Relative position of absorption components or a steep wing of Hα.
[f] Relative infrared excess, as compared to the regular photospheric IR flux.

correlate with Hα in our sample, in contrast to the situation for the active stars in Figure 16 of Cohen and Kuhi (1979). Again, the [O I] fluxes of Cohen and Kuhi's objects are larger by up to a factor of 100.

The profile shape of [O I] 6300 Å was used by Appenzeller, Jankovics, and Östreicher (1984) and Edwards *et al.* (1985) to probe macroscopic flow patterns in the circumstellar environment of T Tauri stars. If the position of the stellar line is different from the one of the telluric component, it can be easily used for a kinematical analysis of the envelope, even if the night sky line is not removed from the data. Table 5 shows a general good agreement of the stellar [O I] velocity with the systemic value derived from photospheric lines. No blueshifted stellar emission could be detected in the target stars, except for Sz 98. There, a much more complex profile with a markedly blushifted emission component is present. This velocity of about -80 km s^{-1} coincides well with the position of absorption components in hydrogen, calcium, and sodium. Together with the presence of redshifted components in the sodium lines, this fascinating object shows signs of infall and outflow at the same time. Further observations of Sz 98 will be necessary to establish the variability of these remarkable features. In order to show at which distances from the stellar surface the lines are formed, detailed modeling is required. It should be kept in mind that Sz 98 also has an excessive far-IR flux equalling in strength the observed photospheric radiative losses of this star.

d) Correlations

In this section we discuss the dependence of the Ca II H, calcium triplet, Hα, and Li I line strengths as a function of the Ca II K flux. The chromospheric emission lines of ionized calcium, and in particular H and K, are considered a measure of stellar activity. Here, we will use the surface fluxes F_λ (related to R by $R_\lambda = F_\lambda/\sigma T_{\rm eff}{}^4$; Noyes *et al.* 1984). If we were to normalize F_λ to the "photospheric" stellar luminosity per surface area $L_{\rm ph}/4\pi R_*{}^2$, typical values for $R_{\rm H\,K}$ range from 7×10^{-4} to 1.4×10^{-3}. Compared with active dwarf stars (Noyes *et al.* 1984), the T Tauri stars investigated here are more active by about 2 orders of magnitude.

It may not be surprising that analyses of even more active stars (e.g., Hartmann *et al.* 1986) for correlations between line fluxes and stellar rotation tend to yield much less clear results than for main-sequence stars. One should keep in mind that for active stars the Ca II or hydrogen emission lines may have an envelope contribution which is not necessarily related to surface activity (distinguishable only at high spectral resolution). The envelope emission may be hiding a clearer relation involving just the surface activity. The main point is that it is possible to separate the surface and envelope contributions when line *profiles* are available.

On the other hand, one must consider the possibility that the surface activity and envelope emission are actually related to each other somehow. We find a good correlation between log F(Hα) and log F(Ca II K) (Fig. 6*a*). This is also true for Hβ, leading to a fairly constant Balmer decrement as discussed above. The much larger sample of Bouvier and Bertout (1986*b*) smoothly extends this trend to objects with higher surface fluxes. This is a rather remarkable result, since it is already obvious just from looking at the kinematic structure of the K-line compared to Hα that the two lines are formed in quite different parts of the atmosphere. Studies of model atmospheres (Calvet, Basri, and Kuhi 1984) confirm that this is likely the case. It is hard to see why a strong correlation between the two should exist unless a common physical phenomenon is responsible for both. For example, if the envelope emission in Hα arises due to a wind which is driven by Alfvén waves as suggested by Hartmann, Edwards, and Avrett (1982) and the Ca II flux is directly related to the surface magnetic fields, they might both vary as the magnetic field varies. If the envelope emission were dependent on processes in a surrounding disk, on the other hand, such a connection would be rather surprising. In this regard, it is instructive to consider the case of the "naked" T Tauri stars, as discussed by Walter (1986). Two of the stars here, Sz 68 and Sz 65, lie within that regime. Our results indicate that stars can be found in all states of undress, and that the relation between Ca II and the Balmer lines holds throughout. It is also clear that these stars are not fully naked, since the Hα line *profiles* are not purely chromospheric even though it would be possible in principle to produce the emission flux observed from an active stellar surface. The question of the connection between these two important lines is clearly worthy of more investigation.

If one considers the calcium H line flux (corrected for a contribution of Hε) versus K line flux, a direct proportionality

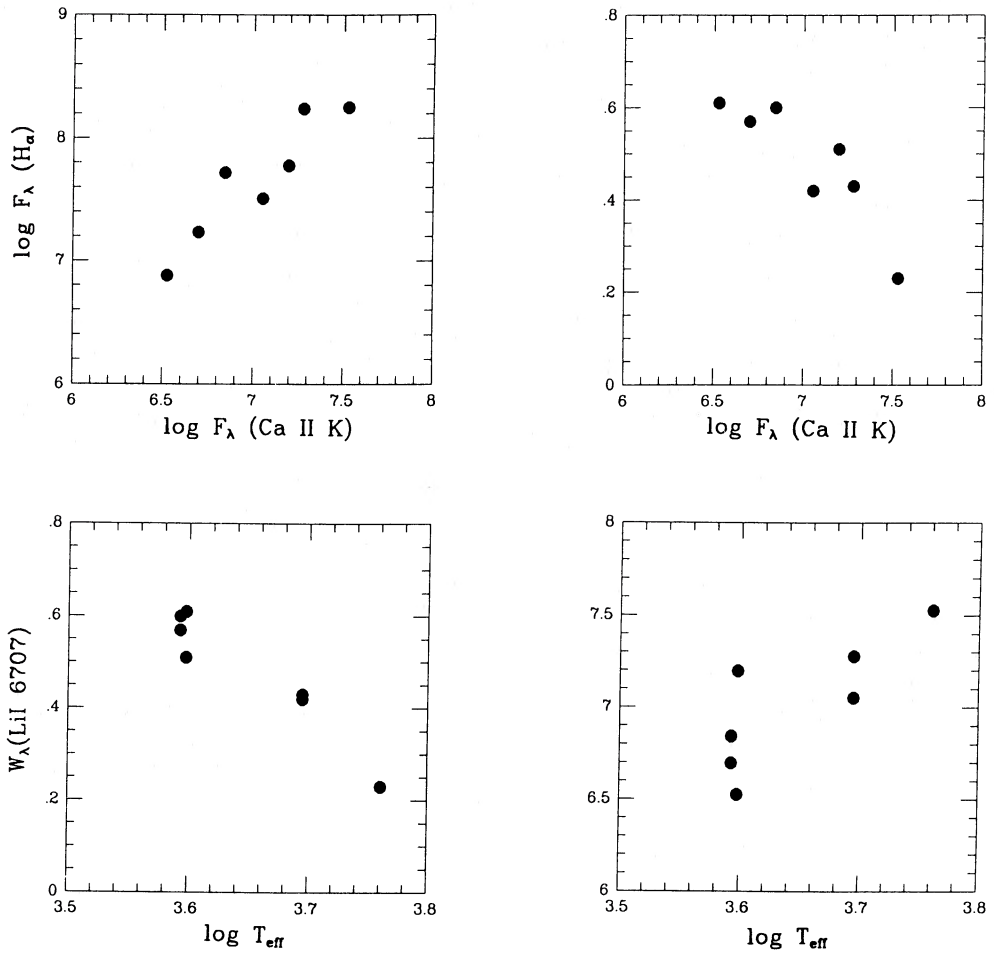

FIG. 6.—Correlations of (*top left*) Hα vs. Ca II K, (*top right*) Li I 6706 vs. Ca II K, (*bottom left*) Li I 6707 vs. T_{eff}, and (*bottom right*) Ca II K vs. T_{eff}

results. Both lines are equally strong for most of our T Tauri stars (Table 2). Since the K line has an oscillator strength twice as big as the H line, one would expect a ratio of 0.5 in the simple optically thin case. Only Sz 98, our peculiar object, obeys this law. The comparable line strength of the K and H lines is also reflected by their same height in Figure 2. Presumably, both lines have a source function which is almost identical for the two transitions.

The infrared calcium triplet lines show the same behavior as the ultraviolet calcium lines (Table 2). No correction was incorporated in order to account for a contribution by the higher lines of the Paschen series, since the adjacent Paschen lines were barely visible at all. If the H and K lines obey a ratio of unity, then the triplet lines do so, too. Again, Sz 98 is the exception. In addition, this object is the only one with a circumstellar absorption component in the calcium triplet lines at 48, 40, and 45 km s^{-1}, respectively. Linsky *et al.* (1979) have noted the close correspondence between the triplet lines and the resonance lines in main-sequence stars, and since they share upper levels, this is not unexpected.

Herbig and Soderblom (1980) have pointed out the unit ratio for more active T Tauri stars. They interpreted their findings as being due to emission from optically thick, localized regions and pointed out the similarity with solar plages. An alternate way to look at the problem is to apply the Eddington-Barbier relation (see below) to ionized calcium. If the source function in the chromosphere has a common numerical value for both the H and K line at optical depth unity for each line, equally strong lines will result. The chromospheric temperature plateau confirmed by Calvet, Basri, and Kuhi (1984) supports this view.

Another puzzling finding in our data is illustrated in Figure 6 (*upper right*), where the equivalent width of Li I 6707 is plotted versus the K line flux. Clearly, the stronger the K line, the weaker the lithium line strength. Though interesting, this dependence should be viewed with caution since it also appears that the lithium line strength is a function of the effective temperature as shown in Figure 6 (*lower left*). However, the Ca II surface flux is *not* related in a simple way to effective temperature (Fig. 6 [*lower right*]). A statistically more representative sample needs to be analyzed before a general conclusion can be made. Giampapa (1984) has argued that on the solar surface increased nonradiative heating is to ionize lithium. The inverse proportionality of lithium line strength and Ca II K emission line flux found for our T Tauri stars qualitatively supports this view subject to the same caveat about temperature. If the same holds true for T Tauri stars as a whole, the lithium line strength is suspect as an unambiguous measurer of youthful stellar age and one must wonder about the cooler old stars as well.

V. THE PHOTOSPHERIC SPECTRUM

In this section we use the observational material presented above for a quantitative comparison between the spectra of T Tauri stars and their associated inactive templates. The approach to study the difference is to consider the flux ratio or flux difference of the active relative to the quiet object. This technique utilized by Linsky *et al.* (1979) for the infrared triplet of Ca II. It was applied to the photospheric spectrum of T Tauri stars by Strom (1983) but without much elaboration. Our data are particularly well suited for this purpose since it is at high resolution, is flux-calibrated, covers a very wide wavelength interval, and was obtained with a linear detector at good signal-to-noise ratio. The underlying assumption for this technique is always that the stellar atmosphere of the program star and the standard resemble each other sufficiently that a direct comparison is meaningful. This is often taken to mean that they resemble each other at large optical depths, while the surface or extended parts of the atmosphere might be different. One can easily get a spurious ratio signal if the broadening mechanisms are sufficiently different, the temperature structures are never homologous, or the line formation physics is sufficiently different due to a variety of factors such as gravity, abundances, atmospheric inhomogeneities, and so on. The technique is only really useful, therefore, if a null signal can be demonstrated for some cases. This gives confidence that the underlying assumption of similarity is really a reasonable one.

a) Technique

We have considered whether to present differences or ratios. Difference plots are only meaningful when made between spectra with continua normalized to the same value. This is the case here for wavelengths longer than about 5700 Å. As can be seen from Figure 2*b*, shortward of 5700 Å it is increasingly difficult to determine the true continuum. For this region only ratio plots can be analyzed. We compared ratio and difference representations of the red data and found no qualitative differences except that ratio plots enhance the contrast when the flux at line center approaches zero in the standard star.

Before comparison, the standard stars (which are all slow rotators with $v \sin i$ values below our detection threshold) had to be convolved with a rotational function in order to match the $v \sin i$ of the T Tauri stars. The expression from Gray (1976) was used, assuming a limb darkening coefficient of 0.6 and the $v \sin i$ from Table 4. The fact that the lower photospheres of the T Tauri stars are observed to be very similar to the standard stars justifies this treatment of limb darkening (which is a second-order effect anyway). Another adjustment is a shift in wavelength to account for the different rest frames of the two photospheric spectra. This value was provided by the position of the cross-correlation peak available from the determination of the systemic velocity as described above. Unfortunately, this wavelength shift also affects telluric lines, which already are in the same frame. If these lines are also rotationally broadened in the standard star then they do not properly cancel the sharp lines in the target spectra. Ideally, telluric lines should be removed ab initio, a task which is hard to accomplish in spectra with this dispersion. For these reasons no corrections were made for telluric lines, but when interpreting ratio plots their influence should be kept in mind. Fortunately this is not a major concern in practice.

The technique described above was illustrated previously (Finkenzeller and Basri 1985, their Fig. 2), where a nonrotating standard star, the same star convolved with a rotational function, a T Tauri star, and the direct ratio of these is plotted. A striking feature of all the ratio plots is the high degree to which weak and medium strength photospheric lines divide out (Fig. 7 [Pl. 8]). Apart from lines where emission is expected anyhow (e.g., the hydrogen and Ca II lines), some of the stronger absorption features in the T Tauri star appear to be shallower than in the standard star. In particular, this is the case for lines of Fe I (42), Fe I (43), Ca I, Mg I, and others. It is exactly these lines which are in emission in strongly active T Tauri stars. Ratio or difference plots of intermediately active T Tauri stars thus indicate the same physical phenomenon as in their more active counterparts. It is also gratifying to note that the ratio spectra of Sz 19 closely resemble a solar chromospheric limb spectrum. The "trailed plate" chromospheric spectrum shown on Figure 7 (*top*) was obtained during the total solar eclipse in 1905 (Campbell and Menzel 1931). The same physical phenomenon may clearly be inferred for the T Tauri stars in the lower part of Figure 7 (a temperature increase in the upper stellar photosphere) without the help of the occulting disk of the Moon or any spatial resolution!

There are a number of convincing arguments that the observed flux enhancements in the ratio plots are real features and not artifacts of an erroneous zero level. The most worrysome effect in this context is stray light in the spectrograph. This becomes an increasing problem as the orders crowd together at shorter wavelengths in CASPEC. Extreme care was exercised when the interorder background on the echelle frames was fitted by a two-dimensional polynomial, the level of which was subtracted from the data (see Ponz 1986). Any errors inherent to a particular location on the chip would also be averaged out by the subsequent order merging. In addition, the following arguments support the reality of the features:

1. The described phenomenon of filling in of emission lines was noted earlier (Cram 1979; Strom 1983; Calvet, Basri, and Kuhi 1984) and is expected for theoretical reasons. Its observational verification is not a surprise.

2. For adjacent absorption lines of equal depth (e.g., between 4060 and 4080 Å), some show up in the ratio, while others do not, indicating that the effect is not due to the zero level. No virtual absorptions are observed (except in the Balmer lines of Sz 68), arguing against random noise which would lead to emission sometimes and absorption sometimes.

3. When dividing the low-resolution IDS scans of the T Tauri stars by the appropriate standard stars from Jacoby, Hunter, and Christian (1984), the same result is qualitatively obtained at low resolution as in the high-resolution spectrograms: the Balmer, Ca II, and Mg I lines show up in virtual emission. We also see similar results when dividing an active T Tauri star by an inactive one.

4. The effect is unambiguously present at wavelengths where stray light is not important, e.g., for the magnesium triplet at 5180 Å.

5. Completely independent control observations for selected lines of a few northern hemisphere T Tauri stars, carried out by the authors with the coudé spectrograph at Lick Observatory in 1986, show the same phenomenon.

6. Since the T Tauri stars have a lower gravity than the main-sequence standards, one might naively expect their photospheric lines to be narrower and deeper leading to virtual absorption features which are not observed.

Since T Tauri stars represent the most active among the group of cool stars where nonradiative processes play a key

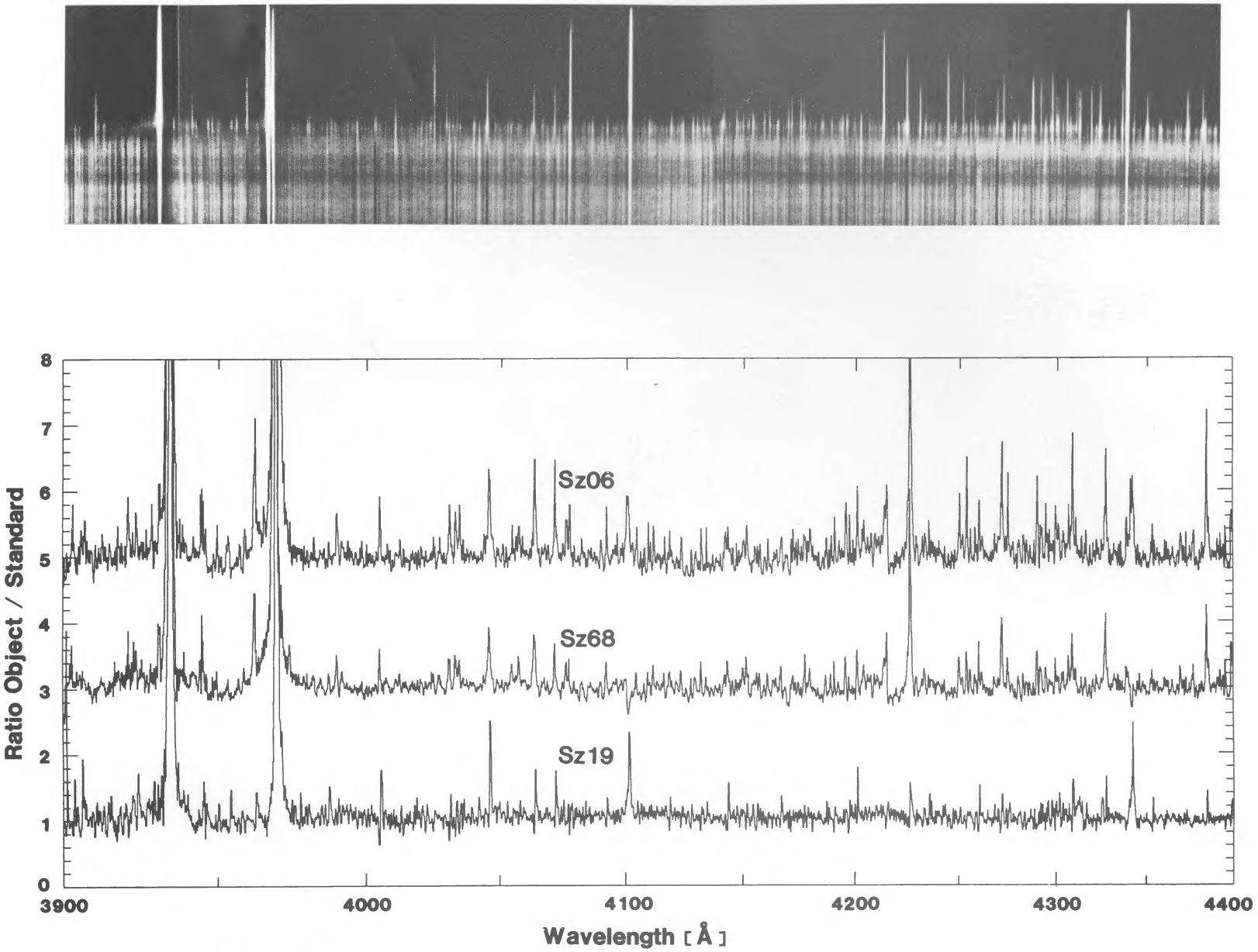

FIG. 7.—Comparison of the ratio plots for the three earliest type T Tauri stars with a chromospheric limb spectrim of the Sun. Note that Sz 19 is G2, but the other are K2 stars. One might expect qualitative, but not quantitative, agreement between the chromospheric spectra.

role in the outer atmosphere, one might suspect the existence of higher macro- and/or microturbulent line-broadening terms than in main-sequence stars. A higher turbulence tends to desaturate the line centers. Fortunately, for microturbulence alone one does not expect a significant effect in the stronger absorption lines. On the other hand, macroturbulence might be a line-broadening mechanism on the order of the stellar rotation for the slower rotators. As shown by Gray (1976), it can be difficult or even impossible to differentiate between a rotational or macroturbulent term in the line profile, even at high resolution and S/N. This effect is of more concern for the determination of $v \sin i$ than for its effect on a differential spectral comparison.

c) *Results*

i) *Continuum Energy Distribution*

The ratios of the low resolution IDS spectrograms relative to the standard stars (after reddening corrections are applied) also allow a comparison of the intrinsic continuum energy distribution of the T Tauri stars in our sample. In the most general case, one would expect an altered continuum level in the blue ("veiling") and at near-infrared wavelengths (thermal dust emission). For the objects considered here, neither excess can be verified in the spectrograms of Figure 1.

The phenomenon of veiling in the blue spectra of T Tauri stars encompasses both an excess continuum level and the apparent weakening of photospheric lines (both relative to the appearance of main-sequence stars at the presumed effective temperature). For more active T Tauri stars it is well known that a blue continuum excess can contribute significantly to the stellar photospheric continuum at wavelengths shorter than about 4200 Å. All stars which show this phenomenon are characterized by optically thick active outer atmospheres, which increasingly mask the underlying photospheric lines. In contrast, the targets in the present study were selected explicitly on the basis of low overall activity and easily discernible photospheric spectral types. It is not very surprising that we find no evidence of an excess with them. Nonetheless one characteristic of veiling, namely the filling in of strong lines, is already present.

Almost all T Tauri stars have a near-infrared excess, due to thermal emission of circumstellar dust. For a typical T Tauri star with a dust temperature of about 1500 K, it is easy to show that shortward of 8000 Å the flux contribution of dust to the stellar photospheric continuum is negligible. The fluxes in Figure 1 therefore represent the true stellar photospheric distributions.

ii) *Line Fluxes*

The fact that no ultraviolet or near-infrared excessive continuum contribution is present in the T Tauri stars of our sample justifies the approach of direct ratios described below. Illustrative ratio plots for wavelengths shorter than 5700 Å are given in Figure 7 for three intermediately active stars, namely Sz 19 (G2), Sz 06 (K2), and Sz 77 (M0). As mentioned above, the most dominant features are the lines of Ca II, Ca I, hydrogen, Mg I, and Fe I multiplets 41, 42, 43. It is obvious that the S/N decreases markedly below 4300 Å. Three important lines in the near infrared are the calcium triplet lines at 8498, 8542, and 8689 Å which share common upper limits with the ultraviolet Ca II H and K lines. These strong infrared lines show up in pseudo-emission, with line profiles closely resembling each other for a given star. These have the same behavior as the results in Linsky *et al.* (1979) but are significantly stronger and sometimes appear in emission even without the ratio having been taken. The lines of Sz 98 appear to show an envelope contribution as well.

Since most of the lines with higher excitation potential fall into the blue wavelength regime, a natural consequence is that fewer virtual emission features are apparent at red wavelengths. Also, as can be seen from Figure 2, the line depth generally decreases toward the red, making a differential filling in more difficult to observe. Finally, the intrinsic contrast between the Planck function at different temperatures (or equivalently a line core and the continuum) is smaller at longer wavelengths. As one moves to cooler objects the changing underlying photosphere results in an enhancement of different lines of other elements and ionization stages. For example, in the case of Sz 77 (M0) the three Mg I lines at 5180 Å have disappeared completely, whereas other lines are enhanced. It is gratifying to note that the strongest features in the ratio plots for Sz 19 (G2) are all notable contributors to chromospheric radiative losses in the Sun (e.g., Withbroe and Noyes 1977). The available material allows the determination of excessive radiative losses in different lines. Due to the vast amount of data and the fact that such an undertaking is only useful in conjunction with detailed atmospheric modeling, we postpone this effort to a later paper in this series.

c) *Interpretation*

One qualitative explanation of the observed behavior of the strong lines is straightforward: strong lines probe a region further out in the stellar atmosphere and the effect is due to a differential increase of the source function in this region, as compared to the inactive standard star. This can be seen by applying the Eddington-Barbier relation which equates the emergent flux at a given wavelength and angle to the numerical value of the source function at the particular optical depth $\tau = \mu$, where $\mu = \cos(\theta)$: $I_{\nu,\mu} = S_{\nu,\tau=\mu}$ (see Finkenzeller and Basri 1985 for a graphical representation). Thus, the residual intensity at the core of each line reflects the value of this source function at approximately unit line center optical depth in each line.

The fact that the weak lines are absent in the observed ratio spectra shows that deep in the atmosphere of a T Tauri star the physical conditions approach the ones in "normal" stars. If we suppose that for T Tauri stars the source function becomes relatively greater than "normal" as one moves outward above a certain optical depth, then lines which become optically thin below that point will look the same in both stars. Lines formed above that point will have brighter cores. Thus, the depth of formation of lines which just begin to show up in the ratio plot is the depth at which the atmosphere of the T Tauri star is significantly heated relative to its main-sequence counterpart. The comparison of ratio plots from different stars can be used to characterize their activity level and atmospheric structure. It is interesting to note that LaBonte (1986) gives ratio plots of active solar regions versus quiet solar regions and quantitatively sees the same phenomenon as in our disk-integrated spectrograms of T Tauri stars.

Of course, the use of the Eddington-Barbier relation is an oversimplification of the real problem: there are always contributions from other optical depths, in particular when an extended envelope is present. Also, the assumption from which the relation follows, namely a linear increase of the source function, is certainly not valid everywhere in the atmosphere.

Finally the direct relation between source function and atmospheric temperature is only valid in LTE. In addition to these problems, the optical depth scale itself is subject to temperature perturbations. The population of the lower level of a transition can be increased or decreased by a temperature increase, depending on its excitation potential and the behavior of coupled levels. The ionization stage relevant to the transition may also change relative to adjacent stages. These changes in population will move the depth of formation of the line and may also affect the wings and core differentially. It is therefore dangerous to take a naive interpretation of the ratio spectra too far. Their utility lies in the demonstration of the basic effect and the identification of which elements and transitions are useful for more detailed analysis.

Despite these problems, there are still some interesting points to be discovered immediately. There is a pattern to the lower state excitation potentials of strong lines which do or do not appear as pseudo-emission features. Certain of the strong lines which do not appear have ground-state excitation potentials which are larger than 3.5 eV. These lines are probably formed deep in the photosphere (where the temperatures are sufficiently high). There are a few resonance transitions which do not fill in [e.g., Sr II 4077 Å and Fe I (3) 4216.2 Å]; a similar explanation may hold for these. The higher densities deep in give the gas a greater heat capacity, so the gas temperature changes will be smaller for the same heating rate. The lines which do show up tend to have lower levels in the 1.0–2.7 eV range. The highest lower levels are for the Mg I B lines. One must be careful of the abundance and strength of these transitions as well as their excitation potential in assessing where they are formed. The Fe I multiplets which show up have lower states at roughly 1.5 eV. Obviously, detailed calculations are required to understand a particular line. The strongest lines (Ca II H and K, Ca I 4226 Å, Balmer lines) which have equivalent widths of 1 Å or more in the Sun have cores which are actually formed near or above the temperature minimum. It is obvious why these lines are strongly filled in since the temperature structure is increasingly perturbed at those heights. The depth of formation of the deepest ratio features identifies the point in the atmosphere where significant nonradiative energy begins to be dissipated. This point is much deeper in the T Tauri stars than in main-sequence stars, presumably because there is much more energy to be dissipated. The surface fluxes of excess emission are also much greater. A detailed examination of the height dependence of the excess will provide an incisive test of heating theories for these atmospheres.

As one examines stars with cooler effective temperatures than the Sun, the strength of the pseudo-emission features appears to increase. For *chromospheric* lines this is expected, since the chromospheric temperature plateau is fairly independent of the effective temperature of the underlying photosphere leading to increasing contrast for cooler stars. It is less obvious that this should be the case for the *photospheric* features; but our results imply that the heating rate in the photosphere is not a linear function of effective temperature and that the contrast between a heated and unheated atmosphere increases for cooler photospheres as well. In the coolest stars we also see emission "bands" in the ratio spectra which are likely due to molecular features. Because of the great sensitivity of such features to atmospheric temperature we are cautious about the interpretation of these. We prefer to wait until more closely matched standards are studied before deciding if these effects are due more to temperature or molecular abundance differences between program and standard stars.

Finally, we note that this sort of analysis need not be confined to pre–main-sequence stars. These are the most active stars (with surface fluxes in UV resonance lines exceeding those of the Sun by up to a factor of 1000), and their late spectral types enhance the effect as well. Even so it is possible that similar effects can be detected for the photospheric lines of active main-sequence stars as well. This will probably require very high signal-to-noise ratios, but the advent of efficient echelle spectrographs and sensitive linear detectors makes the observation of many lines together quite feasible. The reward is information on the part of the stellar atmosphere where most of the nonradiative energy is actually dissipated, and sampling of the depth dependence of this heating. Put another way, the number of diagnostics of stellar activity in the visible spectrum can be greatly increased by this technique. If there are different dependencies on stellar parameters for the photospheric heating (for which acoustic heating is still a strong candidate) and upper chromospheric heating (with clear magnetic dependencies), this technique will be quite valuable in sorting them out.

Many people at different places contributed to this work. In particular, we would like to thank the staff of ESO at Chile and at Munich for their gracious help. The final data reduction was performed with the marvelous ANA spectral processing package written by Richard Shine. We anjoyed valuable discussions with Claude Bertout, G. Herbig, L. V. Kuhi, and R. Mundt.

Financial support for this program came from NSF grant AST 84-14811 and the Alexander von Humboldt-Foundation, Bonn-Bad Godesberg, grant FLF-VB2 while U. F. has been a Feodor Lynen Fellow at Berkeley.

REFERENCES

Abt. H., and Biggs, E. S. 1972, *Bibliography of Stellar Radial Velocities* (New York: Latham).
Appenzeller, I., Jankovics, I., and Jetter, R. 1986, *Astr. Ap. Suppl.*, **64**, 65.
Appenzeller, I., Jankovics, I., and Krautter, J. 1983, *Astr. Ap. Suppl.*, **53**, 291.
Appenzeller, I., Jankovics, I., and Östreicher, R. 1984, *Astr. Ap.*, **141**, 108.
Appenzeller, I., Mundt, R., and Wolf, B. 1978, *Astr. Ap.*, **63**, 289.
Bastien, P. 1985, *Ap. J. Suppl.*, **59**, 227.
Bouvier, J., Bertout, C., Benz, W., and Mayor, M. 1986, *Astr. Ap.*, **165**, 110.
Bouvier, J., and Bertout, C. 1986*a*, in *Lecture Notes in Physics*, Vol. **254**, *Proc. Fourth Cool Stars Workshop*, ed. M. Zeilig and D. M. Gibson (Berlin: Springer), p. 132.
———. 1986*b*, in *IAU Symposium 122, Circumstellar Matter*, ed. I. Appenzeller and C. Jordan (Dordrecht: Reidel), in press.
Calvet, N., Basri, G., and Kuhi, L. V. 1984, *Ap. J.*, **277**, 725.
Campbell, W. W., and Menzel, D. 1931, *Pub. Lick Obs.*, Vol. **17**, Part 1.
Cohen, M. 1973, *M.N.R.A.S.*, **164**, 395.
Cohen, M., and Kuhi, L. V. 1979, *Ap. J. Suppl.*, **44**, 734.
Cram, L. E. 1979, *Ap. J.*, **234**, 949.
Edwards, S., Strom, S. E., Heyer, I., and Strom, K. E. 1985, in *Lecture Notes in Physics*, Vol. **254**, *Proc. Fourth Cool Stars Workshop*, ed. M. Zeilig and D. M. Gibson (Berlin: Springer), p. 436.
Finkenzeller, U., and Basri, G. 1985, *Messenger*, **42**, 20.
———. 1986, in *IAU Symposium 122, Circumstellar Matter*, ed. I. Appenzeller and C. Jordan (Dordrecht: Reidel), in press.
Giampapa, M. 1984, *Ap. J.*, **277**, 235.
Gray, D. F. 1976, *The Observation and Analysis of Stellar Photospheres* (Toronto: Wiley).
Hartmann, L. 1982, *Ap. J. Suppl.*, **48**, 109.
Hartmann, L., Edwards, S., and Avrett, E. 1982, *Ap. J.*, **261**, 279.
Hartmann, L., Hewett, R., Stahler, S., and Mathieu, R. 1986, *Ap. J.*, submitted.
Henize, K. G. 1963, *A.J.*, **68**, 280.
Herbig, G. H. 1977, *Ap. J.*, **214**, 747.
Herbig, G. H., and Soderblom, D. R. 1980, *Ap. J.*, **242**, 628.
Herbst, W., Miller, D. P., Warner, J. W., and Herzog, A. 1982, *A.J.*, **87**, 98.

Jacoby, G. H., Hunter, D. A., and Christian, C. A. 1984, *Ap. J. Suppl.*, **56**, 257.
Kuan, P., and Kuhi, L. V. 1975, *Ap. J.*, **199**, 148.
Labonte, B. J. 1986, *Ap. J., Suppl.*, **62**, 229.
Linsky, J. L., Hunten, D. N., Sowell, R., Glackin, D. L., and Kelch, W. L. 1979, *Ap. J. Suppl.*, **41**, 481.
Mundt, R. 1984, *Ap. J.*, **280**, 749.
Murphy, D. C., Cohen, R., and May, J. 1986, *Astr. Ap.*, **167**, 234.
Noyes, R. W., Hartmann, L., Baliunas, S., Duncan, D., and Vaughan, A. H. 1984, *Ap. J.*, **279**, 763.
Ponz, D. 1986, *Messenger*, **43**, 31.
Savage, B. D., and Mathis, J. S. 1979, *Ann. Rev. Astr. Ap.*, **17**, 73.
Schwartz, R. D. 1977, *Ap. J. Suppl.*, **35**, 161.
Strom, S. E. 1983, *Rev. Mexicana Astr. Ap.*, **7**, 201.
Ulrich, R., and Knapp, G. R. 1985, preprint.
Walter, F. M. 1986, *Ap. J.*, **306**, 573.
Withbroe, G. L., and Noyes, R. W. 1977, *Ann. Rev. Astr. Ap.*, **15**, 363.

G. Basri and U. Finkenzeller: Astronomy Department, University of California, Berkeley, Berkeley, CA 94720